

UNIVERSITY OF CALIFORNIA
Santa Barbara

**Comparing Spatially Explicit Models of Fire Spread Through Chaparral
Fuels: A New Algorithm Based Upon the Rothermel Fire Spread Equation**

A Thesis submitted in partial satisfaction of the requirements for the degree of

Master of Arts

in

Geography

by

Marco Emanuel Morais

June 2001

Committee in Charge:
Professor Dar A. Roberts, Chairperson
Dr. David Weise¹
Professor Richard Church
Professor Stuart Sweeney

¹ Project Leader, Prescribed Fire and Fire Effects Research, Riverside Forest Fire Lab, USDA Forest Service, Riverside, California

The thesis of Marco Emanuel Morais is approved

Committee Chairperson

June 2001

June 15, 2001

Copyright by
Marco Emanuel Morais
2001

ABSTRACT

A new raster-based spatially explicit model of surface fire spread through chaparral, HFire (Highly Optimized Tolerance Fire Spread Model), is presented. The Rothermel fire spread equation is used to determine the direction and magnitude of the maximum rate of fire spread into a cell. One-dimensional predictions from the Rothermel equation are fit to two-dimensions using the solution to the fire containment problem and the empirical double ellipse formulation of Anderson. A new technique implemented in HFire, based upon finite fractional distances between cell centers, remedies the problem of distorted fire shapes previously identified as endemic to raster models of fire spread. Model accuracy, sensitivity to fuels, and sensitivity to data resolution were evaluated by measuring the coefficient of areal association (C_A) and the kappa coefficient (κ) for observed and predicted fire spread during two historical events, the 1996 Calabasas Fire and the 1998 Ogilvy Fire. Model accuracy for the reconstruction of the Santa-Ana driven 1996 Calabasas Fire was generally satisfactory and ranged from 0.7348 to 0.5774 (C_A) and 0.3960 to 0.1838 (κ). Model accuracy of the 1998 Ogilvy Fire, which burned under more moderate weather conditions, was more variable and ranged from 0.8461 to 0.0636 (C_A) and 0.1826 to 0.0019 (κ). Fire spread predictions of the extreme event were relatively insensitive to the quality of fuels information and data resolution. The opposite was true of the predictions for a fire that had burned under moderate conditions. This has important management implications for using any fire spread model based upon the Rothermel equation to predict fire behavior in chaparral. In addition, comparisons between HFire and the current US standard fire spread simulator, FARSITE, were also made. The HFire model produced patterns of fire growth that were similar but more accurate than FARSITE in 10 out of 12 trials as measured by the C_A and in 9 out of 12 trials as measured by κ . The comparative speed and efficiency of the raster based code presented here puts into question the

efficacy of using vector-based fire spread models based upon Huygens' Principle in the highly heterogeneous conditions experienced in Southern California chaparral.

TABLE OF CONTENTS

ABSTRACT	IV
TABLE OF CONTENTS.....	VI
LIST OF FIGURES.....	VIII
LIST OF TABLES.....	X
ACKNOWLEDGEMENTS.....	XI
NOMENCLATURE	XII
1.0 INTRODUCTION	1
1.1 CLASSIFYING FIRE SPREAD MODELS.....	2
1.2 APPROACHES TO MODELING FIRE SPREAD.....	3
1.2.1 RASTER MODELS OF FIRE SPREAD	4
1.2.2 RASTER MODELS OF FIRE SPREAD: CONTACT-BASED APPROACH	4
1.2.3 RASTER MODELS OF FIRE SPREAD: HEAT ACCUMULATION APPROACH	5
1.2.4 VECTOR MODELS OF FIRE SPREAD	6
1.3 EVALUATING THE ACCURACY OF THE ROTHERMEL MODEL.....	8
1.4 EVALUATING THE ACCURACY OF SPATIALLY EXPLICIT MODELS.....	9
2.0 HFIRE MODEL DESCRIPTION.....	11
2.1 INPUT VARIABLES REQUIRED FOR PREDICTING FIRE SPREAD.....	11
2.2 FITTING ONE-DIMENSIONAL PREDICTIONS TO TWO-DIMENSIONS	15
2.3 DISTORTION AND THE CELL CONTACT APPROACH	16
2.4 ADAPTIVE TIMESTEP AND FINITE FRACTIONAL DISTANCES	18
2.4.1 EXAMPLE: CELL-TO-CELL FIRE SPREAD.....	21
2.5 TRACKING FIRE EXTINCTION USING CELL STATES	24
2.6 ASSESSING RUN TIME EFFICIENCY.....	25
3.0 HFIRE ACCURACY ASSESSMENT: METHOD & RESULTS.....	27
3.1 1996 CALABASAS FIRE	27
3.1.1 ASSEMBLING INPUT DATA.....	28
3.1.2 ACCURACY OF PREDICTIONS	29
3.2 1998 OGILVY FIRE.....	37
3.2.1 ASSEMBLING INPUT DATA.....	37
3.2.2 ACCURACY OF PREDICTIONS	38
3.3 RESULTS OF RUN TIME EFFICIENCY TESTS	41
4.0 CONCLUSIONS.....	44
4.1 FUTURE WORK.....	46

REFERENCES CITED.....	48
APPENDIX A: FUEL MODEL DESCRIPTION FILE.....	53
APPENDIX B: FUEL PARTICLE SIZE CLASSES AND FIRE BEHAVIOR	54
APPENDIX C: WINDSPEED REDUCTION.....	57
APPENDIX D: ESTIMATING FIRE SPREAD AT ARBITRARY DIRECTIONS	58
APPENDIX E: REGROWTH FILE USED TO GENERATE FUELS MAPS.....	59
APPENDIX F: 1996 CALABASAS FIRE SIMULATION: RAW RESULTS.....	61
APPENDIX G: 1998 OGILVY FIRE SIMULATION: RAW RESULTS.....	64

LIST OF FIGURES

- 2.1 Variables Required For Predicting Fire Spread
- 2.2a Fire spread from A to C via B' or B''
- 2.2b First iteration of cell contact algorithm
- 2.2c Second iteration of cell contact algorithm
- 2.3 Fire spread through a lattice of square cells with eight degrees of freedom
- 2.4 Fire spread into cell (2,1)
- 3.1 Historical (left) and predicted (right) fire behavior at 2100 hours during the 1996 Calabasas Fire using the HFire model. Example of high accuracy. Inputs used during this simulation: Cheesbro RAWS weather data, custom fuels, and 100 meter spatial resolution.
- 3.2 Areas of burned agreement (Region 1), unburned agreement (Region 4), underprediction (Region 2), and overprediction (Region 3).
- 3.3 Historical (left) and predicted (right) fire behavior at 2100 hours during the 1996 Calabasas Fire using the FARSITE model. Example of high agreement between burned areas (R_1), but with large overprediction error (R_4). Inputs used during this simulation: Malibu RAWS weather data, NFFL fuels, and 100 meter spatial resolution.
- 3.4 Historical (left) and predicted (right) fire behavior at 2100 hours during the 1996 Calabasas Fire using the HFire model. Example of high accuracy as measured by κ . Inputs used during this simulation: Malibu RAWS weather data, NFFL fuels, and 100 meter spatial resolution.
- 3.5 1996 Calabasas Fire Cumulative Area Burned, Historical and Predicted (Custom Fuels). Results from HFire and FARSITE trials are shown. Simulation parameters are abbreviated as follows: cust, custom fuels; 30m and 100m, spatial data resolution; mal, Malibu RAWS; che, Cheesbro RAWS.
- 3.6 1996 Calabasas Fire Cumulative Area Burned, Historical and Predicted (NFFL Fuels). Results from HFire and FARSITE trials are shown. Simulation parameters are abbreviated as follows: nffl, NFFL fuels; 30m and 100m, spatial data resolution; mal, Malibu RAWS; che, Cheesbro RAWS.

- 3.7 Historical (left) and predicted (right) fire behavior at 1700 hours on October 22 during the 1998 Ogilvy Fire using the HFire model. Example of severe overprediction. Inputs used during this simulation: custom fuels, and 100 meter spatial resolution.
- 3.8 1998 Ogilvy Fire Cumulative Area Burned, Historical and Predicted. Results from HFire and FARSITE trials are shown. Simulation parameters are abbreviated as follows: cust, custom fuels; 30m and 100m, spatial data resolution.

LIST OF TABLES

- 2.1 Example fire spread scenario
- 2.2 Maximum rate of fire spread out of each cell
- 2.3 Fractional distances for fire spread in each case
- 3.1 Measures of association for the 1996 Calabsas Fire
- 3.2 Measures of association for the 1998 Ogilvy Fire
- 3.3 Run time performance of HFire model during 1996 Calabasas Fire
- 3.4 Run time performance of FARSITE model during 1996 Calabasas Fire

ACKNOWLEDGEMENTS

I would like to thank NASA for funding the creation of the Southern California Wildfire Hazard Center (SCWHC) under the auspices of a Regional Earth Science Application Center (RESAC) Program. Without the funding supplied through the SCWHC this research would not have been possible. I would also like to thank David Weise, Jon Regelbrugge, and Francis Fujioka of the United States Forest Service Riverside Fire Lab for their help, encouragement, and cooperation on several projects developed at the SCWHC. This research was assisted by all members of the Advanced Remote Sensing Group directed by Dr. Dar Roberts at the University of California, Santa Barbara. In particular, I would like to give special mention to Phil Dennison, Dylan Prentiss, Segun Ogunjemiyo, Meg Gardner, and Ernie Reith for their advice and good company over the last few years. Max Moritz and Jean Carlson provided significant input during the development of the HFire model to enable it to be used for stochastic long-term simulations of fire regime. Max Moritz deserves additional thanks for contributing to many of the ideas and features of HFire. Administrative staff at the Institute of Computational Earth Systems Science (ICESS) and the Department of Geography deserve thanks for their conscientious management of the paperwork required to complete this project. Some of the data used during this project not generated at UCSB were provided by the National Park Service and the Los Angeles County Fire Department. Thanks and love to Caitlin and my three cats, Moma, Polly, and Harold, who endured almost three years of only spending weekends together. My parents deserve the most credit for stressing the importance of education and their emotional and financial support. Finally, thanks to Dr. Dar Roberts for continuous support, guidance, encouragement, and patience during this research.

NOMENCLATURE

NOTATION

d	distance, in m
Δd	size along one dimension of square cells in a lattice, in m
h	height, in m
I_R	reaction intensity, in $\frac{J}{m^2 s} = \frac{W}{m^2}$
L	length, in m
Q	volumetric heat content, in $\frac{J}{m^3}$
Q_{ig}	heat of preignition, in $\frac{J}{kg}$
q	heat flux, in $\frac{J}{m^2 s} = \frac{W}{m^2}$
R	rate of fire spread, in $\frac{m}{s}$
s	surface-area-to-volume (SAV) ratio, in $\frac{m^2}{m^3}$
t	timestep, in s
U	windspeed, in $\frac{m}{s}$
W	width, in m
x, y, z	axis of Cartesian coordinate system

GREEK SYMBOLS

E	eccentricity, <i>unitless</i>
ε	effective heating number, <i>unitless</i>
Φ_s, Φ_w	slope and wind factors, <i>unitless</i>

ρ	density, in $\frac{kg}{m^3}$
Θ	azimuth from 0° to 360°
ξ	propagating flux ratio, <i>unitless</i>

SUBSCRIPTS

<i>eff</i>	effective (vected) quantity
<i>f</i>	fuel bed property
<i>fp</i>	fuel particle property
<i>max</i>	condition at maximum
<i>mid</i>	measured at midflame height, halfway between the top of the fuel bed and the top of the flame
Θ	condition at arbitrary azimuth from 0° to 360°
<i>ref</i>	measured at reference height, 6.096 meters above the height of the vegetation is standard in the United States
<i>x, y, z</i>	pertaining to a value recorded along the axis of a Cartesian coordinate system

1.0 INTRODUCTION

There is widespread agreement that fire suppression in forested ecosystems has resulted in abnormally high fuel accumulation, predisposing these systems to low-frequency, high-intensity, large fires. The solution to the threat posed by wildland fire in these areas is to reduce the widespread accumulation of fuels with treatments such as prescribed burning or mechanical thinning. Since 1910, there has been a significant increase in the frequency of fires in chaparral-dominated Central and Southern California, and, in the case of Southern California, a significant increase in the annual area burned by these fires (Keeley, et. al., 1999). The lack of a significant increase in the mean fire size over this time suggests that suppression of wildfires burning through chaparral appears to have had little effect on mean fire size and is less dependent upon fuels accumulation (Moritz, 1997; Keeley, et al., 1999). As a result, a strategy of targeted, rather than widespread, fuels treatment and suppression has been advocated for these systems (Conard and Weise, 1998; Keeley, et. al., 1999). Predictive models of fire spread and the intelligence gathering that they require will be an essential component to executing this strategy effectively.

Interest in predictive models of wildland fire spread has existed more or less continuously since the late 1930s and has produced a substantial body of published information (Fons, 1946; Catchpole and DeMestre, 1986; Weber, 1991; Pitts, 1991). From the perspective of a fire manager working for a land management agency in the United States, the culmination of this accumulated knowledge is encapsulated in the United States (US) fire prediction system. The fire spread predictions used by the current system are based upon a semi-empirical formulation first presented by Rothermel in 1972. This system has been implemented operationally in the form of programmable hand-held calculators in the late 1970s (Rothermel, 1983), the BEHAVE minicomputer program in the middle 1980s (Andrews, 1986), and the FARSITE fire spread model in the middle 1990s (Finney, 1998). FARSITE is unique because it is the first component of the national system which provides spatially

explicit predictions of fire spread. FARSITE can be used during complex wildfire situations, however it was intended to be used under more controlled conditions, such as prescribed fires or prescribed natural fires. FARSITE also incorporates features, such as a crown fire spread module, which maximize its applicability to a diversity of fuel types.

Unlike FARSITE, the design of the HFire (Highly Optimized Tolerance Fire Spread Model) model exchanges flexibility for specialization to the chaparral fire regime. HFire is a spatially explicit model of surface fire spread through chaparral fuels for use in real-time during complex fire situations. Unlike forest fires which can burn for weeks at a time, chaparral fires often burn in a matter of hours or days, and the real-time performance of HFire is better suited than FARSITE to provide rapid predictions during these events. This paper describes the implementation of the HFire model, makes comparisons between fire spread predictions using HFire and FARSITE to observations of historical fire spread, and evaluates the sensitivity of the predictions to the quality and resolution of the fuels and landscape data used.

1.1 CLASSIFYING FIRE SPREAD MODELS

Weber (1991) presents a system of classifying fire spread models based upon the method the model uses to incorporate physical principles. Fully empirical models have no direct connection to physical principles and instead rely on statistical correlation between variables known to influence fire spread. Typically, such models regress rates of fire spread observed in the field against variables such as windspeed, slope, fuel moisture content, fuel bed depth, and fuel load. A weakness of any fully empirical model is that predictions made for fire spreading under experimental conditions that were not explicitly tested for may be unreliable. In contrast, semi-empirical and physically-based models of fire spread estimate the flux between burning and unburned fuel according to the conservation of energy (Equation 1.1).

$$R = \frac{\sum_{m=1}^u q_m}{\sum_{n=1}^v Q_n} \quad (1.1)$$

Under steady-state conditions, the rate of fire spread, R , in m/s, is equal to the ratio of the heat received by unignited fuel ahead of the fire, q , in J/s-m², over the heat required to ignite the fuel at the leading edge of the fire, Q , in J/m³ (Williams, 1976). The total energy flux received by the unignited fuel, q , is equal to the sum of the individual u energy fluxes received due to heat transfer via radiation, convection and conduction. The total energy required to ignite a unit volume of fuel, Q , is equal to the sum of the heat required to bring the individual v components of the fuel bed from ambient temperature to ignition temperature. Semi-empirical models are distinguished from physical models in how each of the u and v components in this relationship are treated. The Rothermel equation (1972), Equation (1.2), is an example of a semi-empirical model. Frandsen (1971) solved for the conservation of energy and Rothermel parameterized it by substituting the summation of the heat transfer terms in q with empirically derived variables.

$$R = \frac{I_R \xi (1 + \Phi_w + \Phi_s)}{\rho_f \varepsilon Q_{ig}} \quad (1.2)$$

In the Rothermel equation, R is the rate of fire spread, in m/s, I_R is the reaction intensity, in J/s-m², ξ is the propagating flux ratio, Φ_w is the wind factor, Φ_s is the slope factor, ρ_f is the fuel bed bulk density, in kg/m³, ε is the effective heating number, and Q_{ig} is the heat of preignition, in J/kg. Although physically-based models of fire spread may provide a more versatile theoretical base upon which to develop predictions of fire spread in spatially explicit models such as HFire, no physically-based operational model of fire spread suitable for this purpose currently exists.

1.2 APPROACHES TO MODELING FIRE SPREAD

Actual fire spread is continuous. The ideal representation of this phenomenon in a computer simulation would employ a system of partial differential equations describing fire spread, or more precisely the change in fuel temperature as a function of time. The location of the fire at any time would be expressed as a continuous temperature field, solved to the desired level of precision, rather than a geometric artifact, such as an arc or a lattice cell, produced from the computer simulation. Such a system of continuous functions has not been implemented in an operational model, resulting in the use of alternative discrete raster and vector models of fire spread. A comparison between the raster and vector approaches highlights the advantages and disadvantages offered by each.

1.2.1 RASTER MODELS OF FIRE SPREAD

Raster schemes of representing two-dimensional fire growth partition the modeling domain into regularly spaced square or hexagonal lattices that restrict the orientation of fire spread to the cardinal axes associated with an individual cell (Kourtz and O'Regan, 1971; Frandsen and Andrews, 1979; Green, et al., 1990; Clarke, et al., 1994). In a raster model, the number of cardinal axes is referred to as the degrees of freedom. In general, higher degrees of freedom afforded by the model should result in less distortion in fire growth (Frandsen and Andrews, 1979), but this has not been empirically proven (French, et al., 1990). The method of simulating fire growth in a raster model can be classified into two general methodologies, contact-based and heat accumulation (Green, 1983).

1.2.2 RASTER MODELS OF FIRE SPREAD: CONTACT-BASED APPROACH

The contact-based approach to fire spread, first presented by Kourtz and O'Regan (1971), is consistent with an interpretation of fire spread as a series of discontinuous ignitions spanning the length of an individual cell. At the start of the

simulation, all cells in the simulation domain are assigned a value of infinity for a variable which tracks the time until the fire arrives. Cells representing ignition points are assigned the current time. Each iteration in the simulation involves a scan of the domain for the cell with the shortest time to ignition. This cell is said to be ignited, representative of an event in the simulation, and the simulation clock is incremented by the amount of time required for the ignition to occur. The advance of the fire from all cells that neighbor ignited cells is also updated if the time required to ignite these cells is less than the time expired during the current event. Since the size of the unit of time that the simulation clock is incremented varies from iteration-to-iteration based upon the timing of an event, the term event-driven or asynchronous simulation is more generally used to describe this class of models (Bratley, et al., 1987). The strength of the approach is that it is extremely computationally efficient because the progress of time is dictated by the rate of spread of the fire, not by a fixed timestep. For fires that spread rapidly, the simulation increments slowly and vice-versa. The weakness of the contact approach is that events are generated based only upon the influence of the single fastest spreading neighbor. Fire spread into a cell that is the cumulative effect of multiple neighboring cells or prior heating is neglected (Green, 1983). French et al. (1990) critically evaluated the performance of several contact based raster models (Kourtz and O'Regan, 1971; Frandsen and Andrews, 1979) and found that the fire shapes produced were severely distorted. These results arose even in cases where the choice of the underlying lattice was varied from a square network of cells to a hexagonal network, effectively increasing the degrees of freedom of the fire spread.

1.2.3 RASTER MODELS OF FIRE SPREAD: HEAT ACCUMULATION APPROACH

The heat accumulation approach to raster fire spread directly addresses the fundamental weakness of the contact-based approach by enabling the rate of spread of fire into a cell to be the sum of the contribution of all neighboring ignited cells

(Green, 1983; Green et al., 1990). In order to do this, the heat accumulation model iterates over fixed time intervals, known as the timestep, continually visiting every cell in the simulation domain and tabulating the quantity of heat received by that cell from all of its neighbors. After receiving some threshold quantity of heat, a cell is considered ignited and begins delivering heat to neighboring cells. The fixed timestep implemented by the heat accumulation approach is representative of a broader class of models known as synchronous simulations (Bratley, et al. 1987). Significant logistical complications arise to ensure that the size of the timestep is large enough to allow the simulation to execute quickly, but small enough that an ignition does not occur at an interval smaller than the timestep. Selecting a fixed timestep is particularly troubling for dealing with fire spread that exhibits a wide range of velocities across the span of the fire front. Furthermore, the phrase “heat accumulation” suggests that there is a physical basis for the method used to describe a cell’s ability to absorb and emit heat. In practice, all implementations to date have used empirical or semi-empirical models of fire spread as surrogates for the physical properties and mechanisms of fire spread (Green, 1990). Educated guesses have been used in lieu of physical principles to determine appropriate threshold values at which a cell is considered "ignited" (Richards, 1988). French et al. (1990) also empirically evaluated the performance of a heat accumulation model (Green, 1983) and found that it was far more computationally intensive than the contact-based approach because of the relatively small elapsed timestep required to capture rapid fire spread. However, the added cost appeared worthwhile because the fire spread perimeters produced from the heat accumulation model were less distorted than the contact-based models.

1.2.4 VECTOR MODELS OF FIRE SPREAD

In the vector approach to modeling fire spread, the fire spread perimeter at any point in time is represented by an infinitely thin arc consisting of a set of n coordinate

pairs, known as vertices, in a Cartesian plane. The only known vector implementations of fire spread to date have relied upon ellipse theory developed by Anderson (1983) and Huygens' Principle. Ellipse theory is used to fit one-dimensional predictions of fire spread to two-dimensions. The procedure used correlates the magnitude of the maximum rate of spread to the major axis of an ellipse whose eccentricity is empirically determined from the local wind and slope conditions during the fire. The rate of spread in any direction is assumed to be a proportion of the maximum rate of spread equal to the dimensionless proportion resulting from dividing the distance from the rear focus to the edge of the ellipse over the distance along the major axis. Huygens' Principle posits that every point on a wave is a source of secondary wavelets such that the envelope formed by the boundary of these secondary wavelets describes the position of the wave at some later point in time. This applies to fire spread if the points along the wave are assumed to correspond to vertices along the fire spread perimeter and the individual wavelets emanating from the vertices are assumed to correspond to the predicted fire spread ellipses (Richards, 1988). The envelope formed by the line tangent to the n fire prediction ellipses defines the leading edge of the fire.

This approach is used by the FARSITE model (Finney, 1998). One theoretical flaw of this approach is that it equates fire spread to a wave-based process, neglecting the recurring issue of interaction among neighboring vertices along the fire front. Other flaws with the model exist. First, the fire "line" is more accurately described as a variably thick fuel temperature discontinuity rather than an arc of infinitely thin thickness. This implies an indeterminate amount of error in the placement of every vertex in the model. Second, the fractal properties of the fire front (McAlpine and Wotton, 1993) prohibit the application of a universal vertex density. In a vector model, the number of coordinate pairs, n , relative to the length of the perimeter, l , dictates the spatial resolution of the predicted fire spread; referred to as "perimeter resolution" in FARSITE. Clarke et al. (1994) observed from historical fire scars that fire perimeter length is strongly dependent upon level of aggregation, or

scale. Therefore, a suitable universal simulation-wide perimeter resolution is elusive. Third, the explicit storage of the fire spread perimeter as a set of vertices introduces the need for rediscrretization of the fire spread perimeter at each timestep in order to resolve fire crossovers and unburned islands. This is a computationally expensive procedure (Richards, 1990), which occupies a significant portion of the computing time used by the FARSITE model (Finney, 1998). In a critical evaluation of a fire spread model implementing Huygens' Principle, French et al. (1990) found that the model performed well except in cases of fire spread under heterogeneous conditions.

1.3 EVALUATING THE ACCURACY OF THE ROTHERMEL MODEL

Previous research has identified several limitations of the Rothermel model that arise from the introduction of the empirical terms used to estimate the parameter q in the conservation of energy. These limitations include: poor model performance in fuel complexes of mixed size classes (Catchpole, et al., 1993); inability to accurately capture the effects of wind and slope on fire spread (Weise and Biging, 1997); and a rudimentary implementation of the influence of live fuel moisture content (Wilson, 1990). Perhaps the most comprehensive laboratory analysis thus far consisted of 357 fires that were burned through four fuel types and under conditions which controlled for fuel bed depth, packing ratio, moisture content and windspeed (Catchpole, et al., 1998). The ultimate conclusion of this study was that predictions from the Rothermel model were “unsatisfactory” and errors were primarily the result of Rothermel’s original assumption that the heat release component of the fire spread model, q , was solely based upon fuel parameters and not environmental conditions. Limited published comparisons to predictions of fire spreading through chaparral fuel beds in the field exist. Van Wilgen et al. (1985) report an $r^2 = 0.772$ ($p < 0.01$) for observed and predicted rates of fire spread in 14 experimental (controlled) fires burning through fynbos, a similar type of Mediterranean shrubland in South Africa. However, the reported correlation coefficient reflects adjustments made to the fuel

model input parameters to improve the reported correlation between observations and predictions. Regardless of the recognized limitations of the Rothermel model, it remains the current standard operational model of fire spread and is used in many fire behavior related applications such as the BEHAVE fire prediction system and the National Fire Danger Rating System (NFDRS).

1.4 EVALUATING THE ACCURACY OF SPATIALLY EXPLICIT MODELS

The accuracy of spatially explicit predictions of fire spread depend upon four factors: (1) the fire spread model employed (empirical, semi-empirical, or physical); (2) the approach used to apply the model in two-dimensions (contact-based, heat accumulation, or Huygens' Principle); (3) the duration of the simulation; (4) the accuracy of the initialization parameters. Arguments made in Fujioka (1985), but not empirically proven, suggest that steady-state models will tend to overpredict the rate of fire spread. As a fire advances in both distance and time it is subject to changes in meteorology, topography, fuel bed moisture, fuel bed composition, quantity, and arrangement. Averaged values of each of these properties neglect the variability that is present during the actual fire event. As a result, the fire is spreading in the simulation under conditions that are far more homogeneous than actually experienced in the field. The importance of the two-dimensional scheme used to model fire spread has already been mentioned. Briefly, the contact-based model has the advantage of being relatively efficient to implement and execute, but produces distorted fire spread perimeters. The heat accumulation approach is more difficult to implement and more costly of computing resources, but produces fire spread perimeters free of distortion. The vector approach seems to offer the same advantages as the heat accumulation model, but suffers when predicting fire spread under heterogeneous conditions. Finally, the duration of the simulation must also be considered when evaluating accuracy because of the tendency for errors to accumulate and compound over time.

Previous attempts at accuracy assessment of spatially explicit models in chaparral have been limited. Stevenson et al. (1974) describe an operational implementation of an event-based fire spread model using the Rothermel model as the basis of the fire spread predictions. The paper concludes with a brief visual comparison, no statistics are provided, of predicted and observed fire spread which shows excellent agreement to a 1973 wildfire in the Santa Monica Mountains, California. Clarke et al. (1994) conduct a statistical comparison between their unique cellular automata model and a prescribed burn in Southern California. The model accuracy is difficult to assess because of the stochastic nature of the model and the fact that the model required calibration to a time series of thermal remote sensing imagery of the fire prior to analysis. Results from 100 trials indicated that 37.5% of all pixels predicted to burn in one of the trials actually burned in the observed data [Note: the authors report a much higher figure of 77.9% accuracy when only pixels that burned in 50% or more of the trials are considered]. Weise and Fujioka (1998) present an interesting approach to accuracy assessment during a reconstruction of the Bee Fire in the San Bernardino National Forest, California. After calculating an “effective rate of fire spread” for every subinterval of time which historical data is available, representative values of the fire prediction variables during each subinterval were found. The representative values were used to calculate estimates of the steady-state rate of fire spread using the Rothermel equation. The relationship between the observed effective rate of spread and predicted fire spread was good with an r^2 of 0.60 ($p < 0.05$).

2.0 HFIRE MODEL DESCRIPTION

HFire (Highly Optimized Tolerance Fire Spread Model) is a raster-based spatially explicit model of surface fire spread through chaparral fuels. The model is written in the C programming language and was designed to run efficiently on a personal computer for use in real-time prediction of fire spread. The Rothermel fire spread equation (Rothermel, 1972) is used to determine the direction and magnitude of the maximum rate of fire spread. Anderson (1983) established an empirical relationship between windspeed and the length to width ratio of fires fit to a double ellipse. The fire containment problem seeks to determine the distance required to completely encircle an elliptically growing fire. Given the eccentricity calculated from Anderson's relationship, rate of maximum fire spread calculated from the Rothermel equation, and a time interval, the solution to the fire containment problem (Albini and Chase, 1980) provides the distance spread by the fire in any direction. The advance of the fire through the simulation domain is restricted to the degrees of freedom of the underlying lattice and reflects the finite distance traveled between the lattice cell centers during a single time interval. The remainder of this section is dedicated to explaining these features in more detail.

2.1 INPUT VARIABLES REQUIRED FOR PREDICTING FIRE SPREAD

The variables required to predict fire spread using HFire can be subdivided into three groups: (1) temporally static fuel variables; (2) temporally static landscape variables; and (3) temporally dynamic environmental variables. Each of these is pictured in Figure 2.1 along with their metric units. In a spatially explicit model of fire spread, temporal variability serves as a useful center of discussion because the potential of each variable to change with location is implicitly implied.

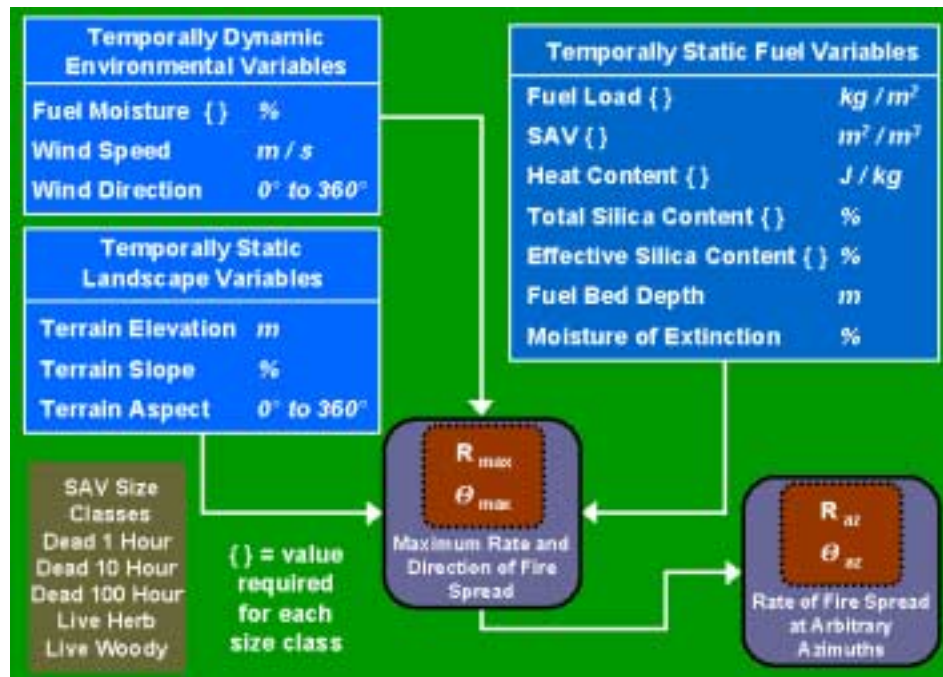


Figure 2.1. Variables Required For Predicting Fire Spread

Although some of the “temporally static” fuel variables listed in Figure 2.1 vary annually due to disturbance and seral stage, the change in these properties during a single fire event is small enough to justify their consideration as constants by the simulation. Instead of supplying raster datasets which explicitly specify the value of each fuel property, HFire accepts a raster of integer fuel model index numbers. A user-supplied fuel model description file (.fmd) cross-references the values of the fuel model numbers used in the raster fuels dataset to a list of fuel properties [see Appendix A]. The format of the file is nearly identical to the fuel model description file used by FARSITE (Finney, 1998). In this way, HFire has the ability to use one of the 13 standard fuel models (Anderson, 1982) or user-defined custom fuel models. Within a single fuel model, some properties, designated with curled braces in Figure 2.1, must be supplied for each surface area to volume (SAV) ratio size class and fuel state (live or dead). The SAV ratio is an important control on fire behavior because the greater the exposed surface of fuel, the more quickly and completely it is brought to ignition [see Appendix B]. Since the Rothermel equation assumes a fuel bed consists of homogeneous fuel particles, a method of averaging these collections of

values is required. HFire uses the SAV-weighting scheme described by Rothermel (1972) to generate a set of “characteristic” fuel bed values.

The temporally static landscape variables (Figure 2.1) may also vary annually due to debris flows and landslides, but the infrequency of these events justifies their consideration as constants. The influence of terrain slope and aspect on fire spread is generally accepted to be a geometric phenomenon. The physical explanation for this is that tilting the ground surface shrinks the angle between the flame standing above the fuel bed and the ground, bringing the unburned fuels closer to the flame. Empirical tests have verified that the Rothermel equation reproduces this effect, at least qualitatively (Weise and Biging, 1997). The terrain elevation is used by HFire to calculate the terrain distance, d_{xyz} , between cell centers represented by the pair of three dimensional Cartesian coordinates $\{x_1, y_1, z_1\}$ and $\{x_2, y_2, z_2\}$ shown in Equation (2.1).

$$d_{xyz} = \sqrt{(x_1 - x_2)^2 + (y_1 - y_2)^2 + (z_1 - z_2)^2} \quad (2.1)$$

Although spatial data are typically stored in planar coordinates, calculating the terrain distance is necessary for tracking fire spread parallel to the ground. Raster elevation data for most of the United States are available in the form of United States Geological Survey (USGS) Digital Elevation Models (DEM). Operators for calculating the slope and aspect from a raster of elevation (z) values are available in most raster-based Geographic Information Systems (GIS). Therefore, HFire requires the user to generate slope and aspect datasets prior to executing the fire simulation code.

The dynamic environmental variables used by HFire differ from the static variables in two ways. First, the simulation assumes that the fuel moisture and the meteorological values read from the input remain constant for *at least* one hour of simulated fire spread before checking for a change in value. This constraint does not reflect a limitation of the internal simulation clock, but was imposed because estimates for these parameters are commonly taken from Remote Automated Weather Stations (RAWS) which report data for one-hour intervals. Unlike FARSITE, the

HFire model does not use user-supplied estimates of temperature and relative humidity to interpolate dead fuel moisture values throughout the day, mimicking diurnal behavior. Instead, the user specified-values of dead fuel moisture are held constant until a new estimate is read from the input; the user is responsible for supplying accurate dead fuel moisture values at a reasonable temporal resolution. This shortcoming is probably not significant for chaparral fire spread because of the tendency for these fires to spread under dead fuel moisture conditions within 10% of zero (personal observation) and the widespread availability of hourly dead fuel moisture estimates from the RAWS. The second difference of the dynamic input variables is that the values can be supplied either spatially or aspatially. For example, a user can specify that a uniform wind speed and wind direction be applied at every cell in the simulation domain during a particular interval of time. Alternatively, spatially varying winds, perhaps generated from a mesoscale meteorological model (Weise and Fujioka, 1998) or a diagnostic wind model (Zack and Minnich, 1991), can also be specified. Spatially varying fuel moisture is currently not available as an operational product, but the use of remote sensing to achieve this is under development and shows promise (Ustin, et al., 1998; Roberts, et al., 1999; Serrano, et al., 2000). The raster datasets of fuel moisture, wind speed, and wind direction used by HFire do not need to be of the same spatial resolution as the static fuels and topography data. Finally, the input wind and weather streams supplied by the user are assumed to be measured at a reference height of 6.096 meters above the top of the fuel bed; the standard for RAWS stations located in the US. The formula given by Albini and Baughman (1979), Equation (2.2), is used to reduce the windspeed using a logarithmic profile to a value typical of what is experienced halfway between the top of the fuel bed and the top of the flame, referred to as midflame windspeed.

$$U_{mid} = \frac{U_{ref}}{\ln \left[\frac{h_{ref} + (0.36h_{mid})}{0.13h_{mid}} \right]} \quad (2.2)$$

U_{mid} is the reduced windspeed, in m/s, at midflame height, h_{mid} , in m, taken from the reference windspeed, U_{ref} , at the reference height, h_{ref} . Rather than explicitly specifying the midflame height, which requires that the flame height is known prior to the prediction of fire spread, all values of windspeed used in HFire are reduced from h_{ref} to a height equal to twice the fuel bed depth [see Appendix C]. This procedure is identical to the custom used in FARSITE for calculating midflame windspeed in nonforested, grass and shrub, areas (Finney, 1998). Although others have identified that a logarithmic windspeed reduction profile may be inappropriate during conditions of local atmospheric instability (Beer, 1990) and during nighttime conditions (Rothermel, et al., 1986), HFire assumes the validity of the relationship holds throughout the duration of the simulation.

2.2 FITTING ONE-DIMENSIONAL PREDICTIONS TO TWO-DIMENSIONS

There is widespread agreement that fire spread under steady homogeneous conditions and in the presence of wind and topography roughly approximates an expanding ellipse. Anderson (1983) describes the length to width ratio of a fire spreading as a double ellipse solely as a function of midflame windspeed. Since Rothermel's original fire spread equation assumes that the wind is aligned directly with slope, the effect of cross-slope winds must be quantified. HFire uses the technique defined in Rothermel (1983) [Figure IV-8] to perform vector addition of the rate of fire spread using no slope and the current midflame wind with the rate of fire spread using the current slope and no wind. From this resultant vector, an effective windspeed, U_{eff} , which defines the magnitude of the effect of the wind in the direction of the maximum rate of spread, is determined. HFire uses a linear approximation of Anderson's (1983) function, described by Rothermel (1991) [Equation 9], to estimate the length to width ratio of an ellipse from the effective windspeed, U_{eff} . Equation (2.3) shows this relationship for an effective windspeed measured in m/s with L equal to the length, in m, and W equal to the width, in m, of the predicted elliptical dimensions.

$$\frac{L}{W} = 1 + 0.5592U_{eff} \quad (2.3)$$

The fire containment problem seeks to determine the final area of a fire given only information about the fire's location, maximum rate of fire spread, and current length to width ratio. Albin and Chase (1980) provide an equation [Equation 6] which gives the final outline of a free burning fire using such information.

$$R_{\theta} = R_{max} \frac{(1 - E)}{(1 - E \cos \Theta)} \quad (2.4)$$

Where the rate of fire spread, R_{θ} , in an arbitrary direction, θ , is calculated as the maximum rate of fire spread, R_{max} , modified by the eccentricity of the elliptical fire shape, E . Albin and Chase (1980) also provide a formula [Equation 8] for determining the eccentricity of the ellipse from the length, L , to width, W , ratio, shown in Equation (2.5).

$$E = \frac{\sqrt{\left(\frac{L}{W}\right)^2 - 1}}{\left(\frac{L}{W}\right)} \quad (2.5)$$

The rate of fire spread in situations of arbitrary wind direction, slope angle (aspect), and directions off maximum is calculated in HFire solely from the relationships presented here [see Appendix D].

2.3 DISTORTION AND THE CELL CONTACT APPROACH

An understanding of why the cell contact approach to fire spread produces distorted fire shapes is helpful for appreciating the improvement achieved using the technique of finite fractional distances implemented by HFire. Figure 2.2a presents a hypothetical situation in which fire can spread from cell A to cell C via one of two intermediary cells, B' or B''.

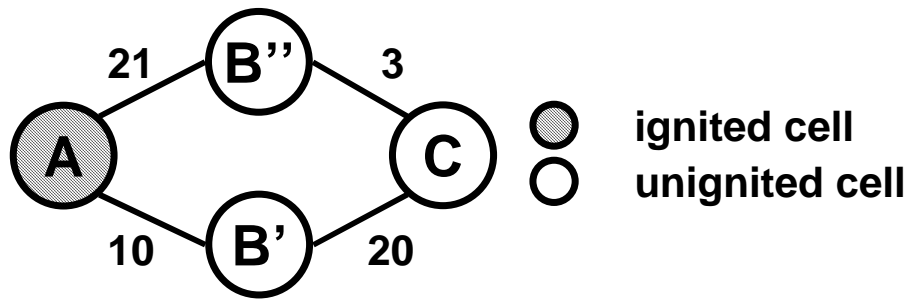


Figure 2.2a. Fire spread from A to C via B' or B''

According to the contact based approach, at initialization cell A in Figure 2.2a will have a time until ignition equal to 0, indicating that it is currently ignited, and all other cells will have a time until ignition of infinity. The cost of traversal, listed adjacent to the edge connecting two cells, represents the time until a fire spreading from a source cell ignites an adjacent destination cell. If the times between every cell in the simulation can be computed a priori, as is shown in Figure 2.2a, then it is apparent that a fire spreads fastest from cell A to cell C by traveling through cell B''. In reality, the conditions affecting the rate of fire spread during the simulation are in constant flux, due to changes in weather, terrain, and fuels, and the cost of traversal between any two cells changes over time. As a result, the algorithm used to calculate fire spread between adjacent cells must wait until the fire has arrived at a particular cell before calculating the rate of spread out of that cell to its neighbors. The costs of traversal shown in Figure 2.2a could not be calculated a priori and are used for illustrative purposes only. Figure 2.2b shows the result of the first iteration of the cell contact algorithm.

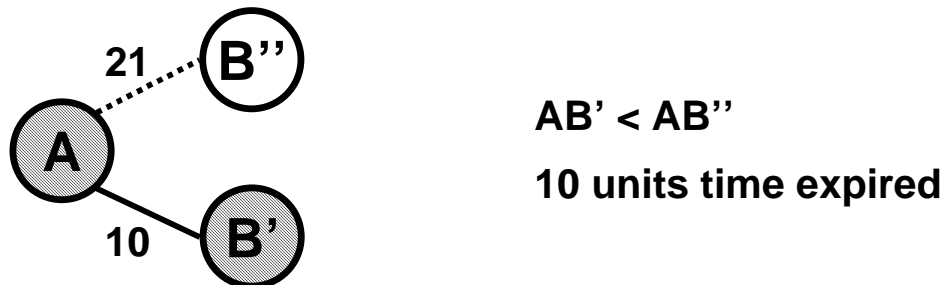


Figure 2.2b. First iteration of cell contact algorithm

By comparing the time until ignition between cell A and B' and cell A and B'', the fire will spread to the cell with the smaller time until ignition, cell B'. Cell B' will

have its time until ignition set to 0, indicating that the fire has arrived, and 10 units of time will have expired during the simulation. Since cell B'' had not previously been visited, its time until ignition will be reduced from infinity to 21 units. Figure 2.2c shows the result of the second iteration of the cell contact algorithm.

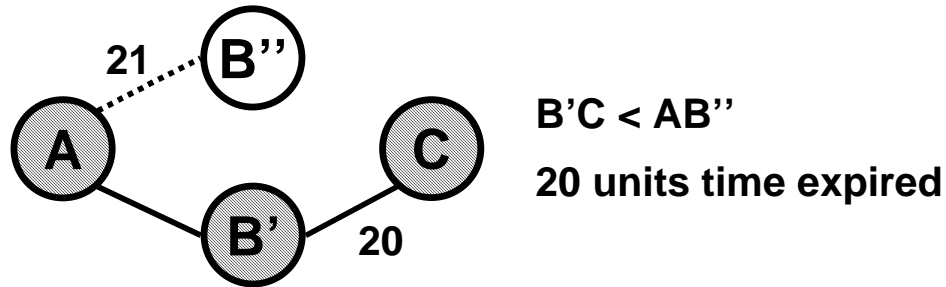


Figure 2.2c. Second iteration of cell contact algorithm

At the start of the second iteration, fire spreading out of two cells is considered, cell A to cell B'' and cell B' to cell C. In the case of fire spread from cell A to cell B'' the conditions influencing fire spread have not changed and a fire spreading between the two would still require 21 units of time to ignite cell B''; the key point being that there is no memory of any heating that may have occurred during the first iteration. Since the time until ignition between cell B' and cell C, 20 units, is smaller, cell C is ignited and has its time until ignition set to 0. Two points emerge from this example. First, an a priori examination of the costs of traversal between cells revealed that the fire spreads fastest by traveling through cells A to B'' to C (24 units of time) as compared with cells A to B' to C (30 units of time). Since the cell contact approach must wait until the fire arrives at a cell before calculating the rate of fire spread out of that cell, the path through a cell of initially high cost, cell B'', was not explored. Second, the effect of prior heating of a cell is neglected. During the second iteration, fire spread between cell A to cell B'' should have reflected some heating of the fuels at cell B'' received during the first iteration. Since the cell contact approach only compares, rather than compounds, the current time to ignition, there is no cumulative effect.

2.4 ADAPTIVE TIMESTEP AND FINITE FRACTIONAL DISTANCES

HFire remedies the problems of distortion in the cell contact algorithm by implementing two features, an adaptive timestep and finite fractional distances. During the discussion below refer to the lattice of square cells, indexed in row-major order and shown in Figure 2.3, where a fire located at the center of cell (2,2) has the potential of spreading to all eight adjacent neighbors. The fire is always said to be spreading out of the central cell (2,2) and into the eight neighboring cells.

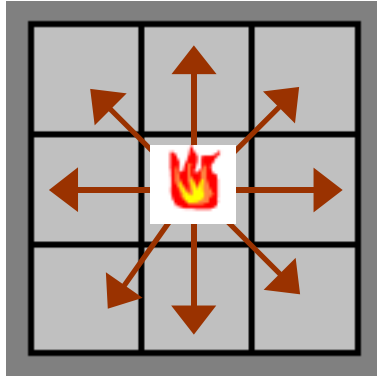


Figure 2.3. Fire spread through a lattice of square cells with eight degrees of freedom

Once the fire beginning at cell (2,2) has arrived at the center of a cell represented by any of the eight adjacent neighbors, the conditions influencing fire spread at the neighboring cell center have the possibility of being different from the conditions at the center of cell (2,2). Therefore, arrival at an adjacent cell center implies that a new rate of fire spread must be calculated. The cell size, Δd , provides a limit on the shortest distance that the fire can travel before conditions affecting the rate of fire spread may change; planar distance along the diagonals will be longer and terrain distance between any cell center will always be equal to or longer than planar distance, except in the case of overhanging terrain. Therefore, the cell size, Δd , divided by the maximum rate of fire spread, R_{max} , yields the minimum amount of time, in s, that can expire in the simulation before the fire may have traveled from one cell center to another. This provides the basis for the size of the timestep used during the n^{th} iteration, t_n , shown in Equation (2.6).

$$t_n = \frac{\Delta d}{R_{max}} \quad (2.6)$$

Since the size of the timestep will change as the fire behavior requires, incrementing more slowly when fire spread is rapid and vice-versa, it is referred to as an adaptive timestep.

The principle behind finite fractional distances, is to eliminate the restriction that fire spreads into a cell from only one direction and during only one timestep. The distance in the direction of a neighbor, d_{θ} , that a fire spreads during the n^{th} iteration is equal to the rate of fire spread in that direction, R_{θ} , multiplied by the duration of the timestep, t_n , shown in Equation (2.7).

$$d_{\theta} = R_{\theta} t_n \quad (2.7)$$

In a more complex situation than is shown in Figure 2.3, fire has the potential to spread into a neighboring cell from many directions. During a single iteration, simply comparing all of the distances and applying the largest to describe the effect of fire spreading into the neighboring cell would be adequate. However, when adding the distance spread during a previous iteration to the distance spread during the current iteration, the potential would exist that the total distance traveled by the fire would exceed the maximum possible distance between a cell and one of its neighbors. As a result, fractional distances are used to normalize the effects of fire spread from multiple directions by the distance parallel to the ground in that direction. In other words, the fractional distance along the segment between the two cell centers is determined by dividing the distance the fire has spread in that direction, d_{θ} , over the terrain distance between the two cell centers, d_{xyz} . During a single iteration, the fractional distance traveled into a cell is compared to a temporary array of fractional distances for that iteration and only the largest fraction is saved. At the conclusion of the timestep, the fractional distances for the current iteration are added to a persistent array of fractional distances. Each cell has only one fractional distance that is meant to represent the portion of the fire having spread the furthest into the cell. Once the fractional distance equals 1.0, the fire has arrived at that cell center, the cell is considered ignited, and fire begins spreading into adjacent neighboring cells.

The adaptive timestep and fractional distance technique presented so far does nothing to preclude the sum of a cell's fractional distance from exceeding 1.0. The adaptive timestep minimizes the occurrence of these cases and the donor cell mechanism, explained below, is used to balance distance overflows when they do occur. In order to establish an accurate estimate of the size of the timestep needed during the current iteration and prevent rampant distance overflow, the maximum rate of fire spread, R_{max} , from all currently ignited cells in the simulation domain is calculated. The maximum of all R_{max} in the domain is used when tabulating Equation (2.6). Whenever a cell's sum fractional distance, stored in a persistent array, exceeds 1.0, the cell becomes a donor of the fractional distance in excess of 1.0. The excess distance is donated to the neighboring cell 180 degrees from the direction in which the fire had spread into the newly ignited cell. For example, if the fire was spreading into the current cell from the southwest, then excess distance will be donated to the cell northeast of the current cell. Since the donor cell has a fractional distance of 1.0, it is considered ignited and fire will begin spreading out of that cell during the following iteration.

2.4.1 EXAMPLE: CELL-TO-CELL FIRE SPREAD

An example of a fire converging on one cell from three neighboring cells is used to complete the discussion of fire spread in HFire. In the example depicted in Figure 2.4, fire is spreading out of cells (2,2), (3,2), and (3,1) and into cell (2,1).

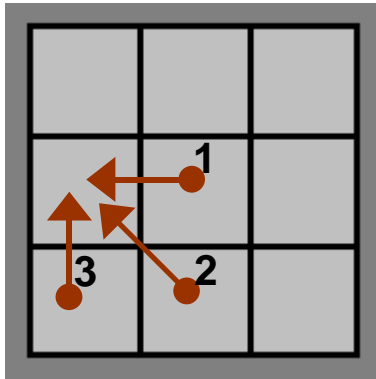


Figure 2.4. Fire spread into cell (2,1)

Table 2.1 shows the variables which describe the situation presented in Figure 2.4. Each instance of fire spread out from one cell and into another has been assigned a case number. By coincidence all three cases have identical values for source cell elevation.

Table 2.1. Example fire spread scenario.

Case	Source Cell Index	Destination Cell Index	Source Elevation	Destination Elevation	Cellsize (Δd)
Units			<i>m</i>	<i>m</i>	<i>m</i>
1	2,2	2,1	200	220	30
2	3,2	2,1	200	220	30
3	3,1	2,1	200	220	30

First, the Rothermel equation, Equation (1.2), is used to calculate the maximum rate of fire spread out of each source cell in Cases 1, 2, and 3. The maximum rate of fire spread, R_{max} , for each case is shown in Table 2.2. The combined effects of wind and slope as calculated from the Rothermel equation produced maximum rates of fire spread at a bearing, Θ_{max} , of 0.0 for all three cases. The cells in this example are assumed to be the only ignited cells in the simulation domain, therefore the max of all R_{max} in the domain is 1.50 m/s, yielding a timestep of 20 s from Equation (2.6) at a cellsize, Δd , of 30 m.

Table 2.2. Maximum rate of fire spread out of each cell.

Case	t_n	R_{max}	Θ_{max}	L/W
Units	s	m/s		
1	20	1.00	0.00	2.0
2	20	1.50	0.00	2.0
3	20	0.75	0.00	2.0

Only Case 3 represents a situation in which the azimuth of the maximum rate of spread, Θ_{max} , is aligned with the direction of spread, Θ , in Table 2.3. Therefore, the rate of spread off-maximum must be determined. From the effective windspeed, U_{eff} , which is not shown, the length to width ratio, L/W, of each predicted fire spread ellipse is calculated using Rothermel's (1991) modification to Anderson's double ellipse using Equation (2.3). For simplicity the length to width ratio for all three cases was set equal. The eccentricity of each ellipse, E, was determined from the length to width ratio, L/W, using Equation (2.5), and ultimately used to solve for the rate of fire spread at an arbitrary direction, R_θ , using Equation (2.4). In each case in Table 2.3, the arbitrary direction, Θ , represents the azimuth from the source cell to the destination cell.

Table 2.3. Fractional distances for fire spread in each case.

Case	θ	d_{xyz}	R_θ	d_θ	d_θ / d_{xyz}
Units		m	m/s	m	
1	270.0	36.06	0.13	2.60	0.07
2	315.0	46.90	0.53	10.50	0.22
3	0.0	36.06	0.75	15.00	0.42

The distance the fire spread from source cell to destination cell, d_θ , was calculated from the rate of fire spread in the direction of the destination, R_θ , and the timestep, t_n , Equation (2.7). The absolute distance, d_θ , was converted to fractional distance by dividing by the terrain distance, d_{xyz} , between the source cell and the destination cell calculated using Equation (2.1). A few additional insights can be gleaned from this table. First, assuming that cell (2,1) had 0.0 fractional distance accumulated at the

start of this iteration, this cell will not be ignited at the conclusion because the largest fractional distance spread was 0.42. Fire spread into this cell during subsequent iterations could occur from any direction and will only require a fractional distance of 0.58 to complete the cell ignition. Second, the cell with the maximum rate of fire spread, case 2, did not spread the furthest distance towards cell (2,1) because of the severe angle between the destination cell and the direction of the maximum rate of fire spread. Third, the cell with smallest maximum rate of fire spread, case 3, ultimately spread the furthest towards cell (2,1) because the direction of the destination cell and the direction of the maximum rate of fire spread were aligned.

2.5 TRACKING FIRE EXTINCTION USING CELL STATES

Fire does not burn inside of a cell indefinitely. In addition to the potential for extinction due to changes in the favorability of conditions for combustion, the fire can also burn itself out by consuming all of the fuel present in the cell. Finite fractional distances only provides the means for accurately describing the ignition of one cell due to another, but not the extinction of fire within a burning cell. Instead, this functionality is provided in HFire through the assignment of one of the four cell states listed below to every cell in the simulation domain.

- Cell is unburnable [U].
- Cell is flammable, but not currently ignited. [N].
- Cell is ignited, but fuel is not consumed. [I]
- All fuel in cell has been consumed by the fire [C].

Unburnable cells [U] correspond to areas without the potential to burn, such as rock outcrops, and water bodies, including the ocean, lakes, and perennial streams. Cells that are flammable, but not yet ignited [N] are distinguished from [I] because they have not yet had fire arrive at their cell center. Consequently, the value of cumulative fractional distance stored in the array index corresponding to these cells ranges from 0.0 to less than 1.0. Cells that are ignited [I], but not consumed, have had fire arrive at their cell center, e.g. fractional distance = 1.0, and are currently spreading fire to

neighboring cells. Finally, all fuel in a cell is considered consumed [C] by the fire in one of two cases. First, if the cell is surrounded only by ignited [I] or unburnable [U] fuel, then the central cell is assigned a consumed state [C]. Cells in this configuration are typically located in the interior portions of an expanding fire. Second, a cell is considered consumed [C] if it has burned longer than a user-specified length of time without propagating itself to all adjacent burnable neighbors. This is implemented in the simulation using a persistent array that tracks the duration since ignition that all cells have been burning. If the cell does not reach the consumed state [C] within the user supplied time, the cell is extinguished and assigned a value of unburnable [U] to prevent future reburns in the area from igniting this cell. The hauling chart given in Rothermel (1983) [Figure IV-1] can be used to select suitable values to assign to this parameter. For example, the hauling chart lists a lower bound on a fire that is worthwhile to suppress at approximately 1 chain/hour (1 chain = 20 meters). This suggests that, in a simulation executing at 100 meter spatial resolution, a fire that does not spread the length of a cell in 5 hours should be extinguished. The description of fuel consumption used by HFire is a gross simplification. However, without a chemical kinetic equation for combustion, the mass loss rate of the biomass involved in combustion cannot be measured and simplifications must be made. Furthermore, there are no implications that cells in the consumed state [C] in the simulation are not undergoing postfrontal combustion, only that the energy released from these cells no longer contributes to the forward rate of spread of the fire. In addition to extinction due to burnout, HFire also implements extinction via a user-defined rate of spread threshold. Any cell which has a maximum rate of fire spread that falls below this threshold is extinguished. Similar reasoning used to set cell consumption limits can be used to set this parameter.

2.6 ASSESSING RUN TIME EFFICIENCY

Run time efficiency is an important attribute of an operational model of fire spread. In lieu of systematic benchmarks, the run time performance of the HFire model was evaluated relative to the current US standard operational model, FARSITE. All comparisons were performed on the same machine with the following configuration, a Pentium III processor with a clock speed of 600 MHz, 256 megabytes (MB) of random access memory (RAM), and 1,000 MB of free secondary storage. All simulations were performed while the machine was idle to ensure fair comparisons and the footprint of each application was examined to ensure that all simulations were executed entirely within main memory.

3.0 HFire ACCURACY ASSESSMENT: METHOD & RESULTS

Simulating historical fire events is a good basis for evaluating the accuracy of spatially explicit models of fire spread. Two historical fires which burned exclusively through Southern California chaparral, the 1996 Calabasas Fire and the 1998 Ogilvy Fire, were simulated. Comparisons between predicted and observed fire behavior were made using the coefficient of areal association, C_A , and kappa, κ (Cohen, 1960). In addition, the sensitivity of the predictions to the quality of the input fuels data used and the spatial resolution of the static landscape variables was also examined. Finally, comparisons between predictions from the HFire model and the current US standard spatially explicit model, FARSITE, were made. The results and conclusions are addressed in detail in the two sections that follow.

3.1 1996 CALABASAS FIRE

The 1996 Calabasas Fire was a Santa Ana wind-driven fire which burned 5159 hectares in the Santa Monica Mountains, California. The fire was actively spreading from the time it started along the 101 freeway on October 21 at 1100 hours until it was contained sometime during the late morning on October 22. The weather conditions under which the fire spread, an average windspeed of 14.3 m/s (32 miles/hr) was measured by a local RAWS at 1100 hours, and consequent fire behavior are representative of an extreme fire event.

At one-hour intervals during the course of the fire, a helicopter equipped with a Global Positioning Systems (GPS) receiver was used to acquire the location of the leading edge of the fire. These data serve as the historical record of fire spread to which all predictions are referenced. The effects of suppression are unaccounted for in the simulation and therefore are a potential source of error in comparing predicted to observed behavior. In this case, fire management personnel attempted to suppress

the spread of the fire, but their effect at the heading portion of the fire was probably minimal because of the extreme winds. However, based upon verbal communication with Herb Spitzer of the Los Angeles County Fire Department, the effect of suppression along the flanks of the fire was measurable and as a result, simulations of the Calabasas Fire that do not account for suppression are likely to overpredict fire spread along the flanks of the fire.

3.1.1 ASSEMBLING INPUT DATA

Historical windspeed, wind direction, and dead fuel moisture data during the fire were available on an hourly basis from two RAWS stations, Cheesbro and Malibu. Both were located no more than 12 km from the fire at any one time. Data from each station were used as input in separate simulations and were not averaged, because of the uncertainty as to which station more accurately reflected the conditions at the time of the fire. Live fuel moisture during the simulation was held constant at a value of 50% of oven dry weight (ODW) for live herbaceous material and 70% ODW for live woody material. These values are representative of seasonal lows for chaparral shrub species, often referred to as “critical”, and reflect the custom established by the fuel modeling component of the BEHAVE system whereby foliage attached to stemwood is tallied as part of live woody fuel moisture.

Use of the most up-to-date map of fuels for the Santa Monica Mountains is inappropriate in a historical reconstruction because the current fuel type in the area of the Calabasas Fire reflects early postfire succession. Instead, a technique was devised to produce a fuels map to reflect the conditions in 1996, prior to the arrival of the fire. First, a map of the potential natural vegetation (PNV), the ultimate floristic composition an area would attain many years after fire, was generated using Franklin (1997). A more detailed species-level map of the Santa Monica Mountains made from imagery acquired immediately prior to the fire was available from Roberts et al. (1998), but was not used because of concerns that differing view geometry during the

acquisition may have introduced error along the seams between north and south image mosaics. Second, the fire history of the Santa Monica Mountains was retabulated to reflect the age of each cell prior to the arrival of the Calabasas Fire. Finally, tables of successional pathways, referred to as regrowth files (.rgr), were used to cross-reference each chaparral PNV type with age to yield a fuel type [see Appendix E]. Two regrowth files, one which exclusively used the standard National Forest Fire Laboratory (NFFL) models and another which included custom chaparral fuel models (Weise and Regelbrugge, 1997), were used to make maps showing NFFL and custom fuels. Since the NFFL does not include a fuel model suitable for describing wildland-urban interface, these areas were designated as unburnable in the NFFL fuel maps. A custom fuel model for describing wildland-urban interface was developed by combining the fuel loadings in the NFFL grass and southern rough fuel models. The wildland-urban interface model was only used in the custom fuel simulations. As in the case of the input weather data, the two sets of spatial fuels data, NFFL and custom, were used for comparison in separate simulation trials.

Terrain elevation for the entire domain was available at 10 meter spatial resolution. Since the spatial resolution of the fuels data was no better than 30 meters, the elevation data were resampled from 10 to 30 meters using bilinear interpolation prior to calculating slope and aspect at that resolution. In order to test for the effect of input data resolution on model predictions, an additional suite of spatial data at 100 meter spatial resolution was generated. The elevation data were resampled to this resolution using bilinear interpolation, slope and aspect were re-generated, and the fuels data were resampled using a nearest neighbor interpolation.

3.1.2 ACCURACY OF PREDICTIONS

Eight simulations of the Calabasas Fire, representing all possible permutations of the weather data sources, fuels data sources, and spatial data resolution, were performed for the HFire and FARSITE fire spread models. Only the first ten hours of

the fire, from 1100 hours to 2100 hours, were simulated because the majority of area burned by the fire was consumed during this time. At the conclusion of each simulation the predicted fire spread was compared to the historical reference data showing the location of the fire front. Figure 3.1 shows the historical and predicted fire spread at the conclusion of the simulation using the Cheesbro RAWS weather data, custom fuels, and 100 meter spatial resolution. This set of input data produced one of most accurate depictions of fire spread and is a useful example for describing the procedure used to assess accuracy.

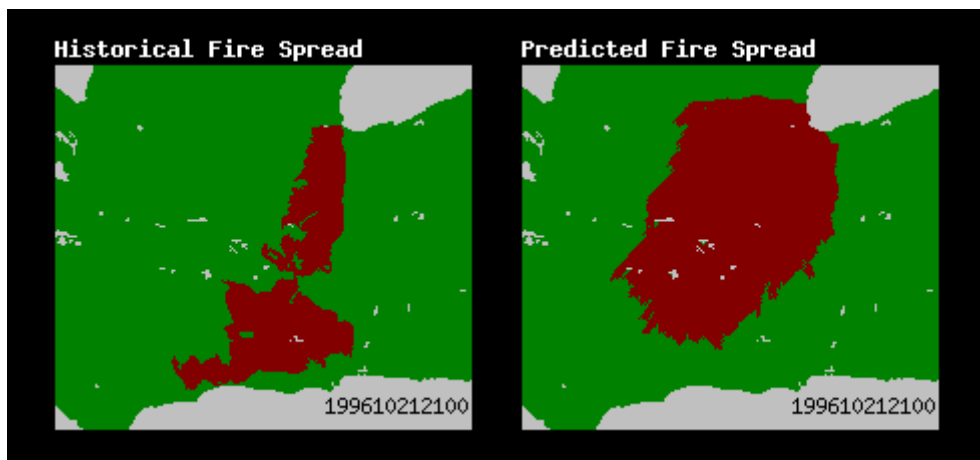


Figure 3.1. Historical (left) and predicted (right) fire behavior at 2100 hours during the 1996 Calabazas Fire using the HFire model. Example of high accuracy. Inputs used during this simulation: Cheesbro RAWS weather data, custom fuels, and 100 meter spatial resolution.

In order to assess accuracy, the area of predicted fire spread was partitioned into the four regions shown in Figure 3.2. Region 1, R_1 , describes areas that both predicted and historical fire spread agreed would burn. Region 2, R_2 , describes areas that were burned in the historical data, but not predicted to burn in the simulation, also referred to as underprediction. Region 3, R_3 , describes areas that were not burned in the historical data, but were predicted to burn in the simulation, also referred to as overprediction. Region 4, R_4 , describes areas that both predicted and historical fire spread agreed would not burn.

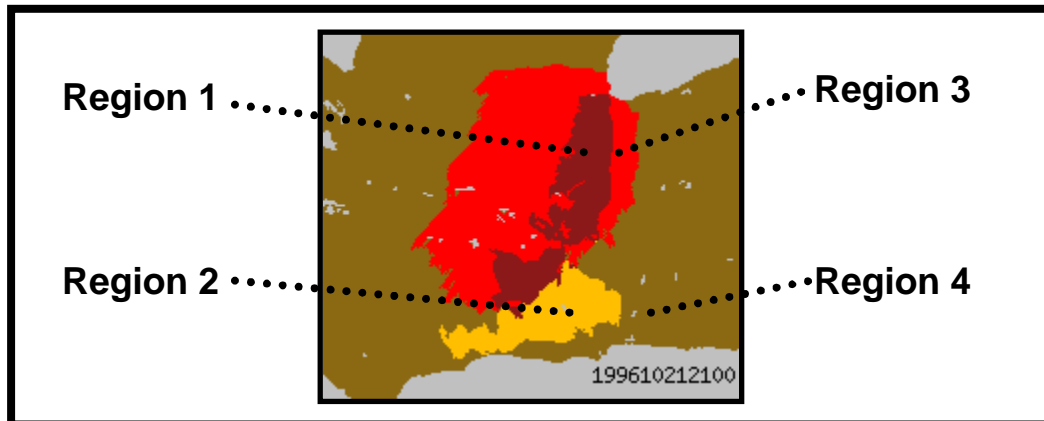


Figure 3.2. Areas of burned agreement (Region 1), unburned agreement (Region 4), underprediction (Region 2), and overprediction (Region 3).

Perfect model accuracy represents predicted fire spread in which all areas are partitioned only into Regions 1 or 4. Errors in predicted fire spread result in nonzero area totals for underprediction (Region 2) or overprediction (Region 3). The total area occupied within each region was tabulated for all eight simulations and three measures of association between predicted and observed fire behavior were calculated. Jacard's coefficient, C_J , measures similarity between maps and ranges from 0.0, completely dissimilar, to 1.0, completely similar, Equation (3.1).

$$C_J = \frac{R_1}{(R_1 + R_2 + R_3)} \quad (3.1)$$

In Equation (3.1), R represents the area occupied by the subscripted region. Note that Jacard's coefficient can sometimes be misleading because it does not include matching unburned areas. The coefficient of areal association, C_A , includes the similarity of both burned and unburned regions, and ranges from 0.0 to 1.0 in the same way as Jacard's coefficient, Equation (3.2).

$$C_A = \frac{R_1 + R_4}{R_1 + R_2 + R_3 + R_4} \quad (3.2)$$

In Equation (3.2), R represents the area occupied by the subscripted region. A good example of the benefit of choosing statistics which include unburned areas as part of the accuracy assessment is shown in Figure 3.3. This simulation, generated from FARSITE, showed a large total area of agreement with the historical data for

predicted burned area, 4003 hectares, but it also had small total area of unburned agreement, 8975 hectares. As a result, the value of Jacard’s coefficient for this simulation, $C_J=0.26$, was equal to the average of all FARSITE simulations, but the value of the coefficient of areal association, $C_A=0.53$, was well below the average of all FARSITE simulations ($C_A=0.62$; $n=8$). The size of the unburned region must be constrained to a reasonable limit, else the value of the coefficient will be a disproportionate reflection of accuracy. In the case of the Calabaras Fire, the extent of the simulation domain roughly corresponds to the maximum predicted extent of the fire after 10 hours of simulation among all models and trials.

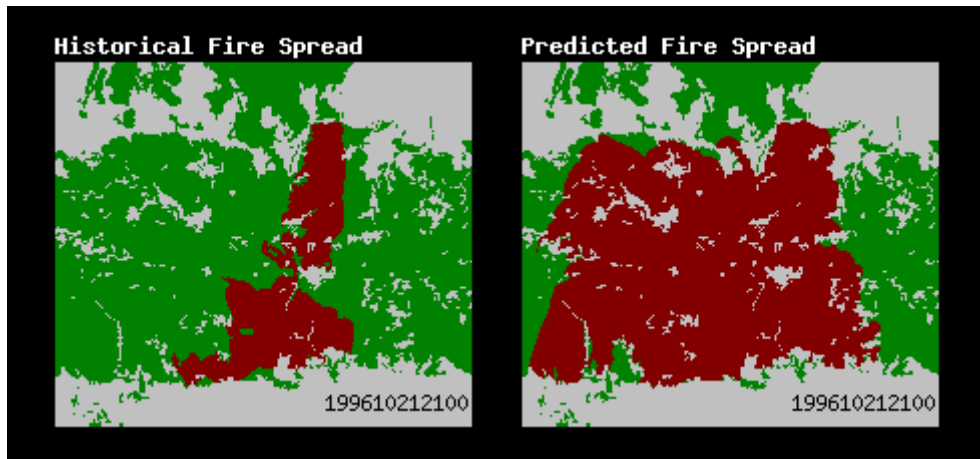


Figure 3.3. Historical (left) and predicted (right) fire behavior at 2100 hours during the 1996 Calabaras Fire using the FARSITE model. Example of high agreement between burned areas (R_1), but with large overprediction error (R_4). Inputs used during this simulation: Malibu RAWS weather data, NFFL fuels, and 100 meter spatial resolution.

The final measure of association used was the kappa coefficient, κ , shown in Equation (3.3).

$$\kappa = \frac{(P_1 + P_4) - (E_1 + E_4)}{1 - (E_1 + E_4)} \quad (3.3)$$

In Equation (3.3), P , referred to as the observed proportion, represents the area of the subscripted region divided by the total area of the simulation domain, and E , referred to as the expected proportion, represents the cross products of the correlation matrix of predicted and observed areas. Unlike C_A , Kappa corrects for the expected area of

association that would occur by chance, and ranges from values of -1.0 , perfect disagreement, to 1.0 , perfect agreement. Values close to 0.0 indicate that the agreement is no better than would occur by chance. All three coefficients have the additional property of being dimensionless, and therefore were used to compare results from maps of different size, but not extent. This feature is important since the wildland-urban interface areas were unburnable in the NFFL fuels data, resulting in an overall burnable area used to compute the measures of association for NFFL simulations that was smaller.

The values of C_A , C_J , and κ , computed for all eight simulations of the Calabasas Fire using both the HFire and FARSITE models are shown in Table 3.1 [see Appendix F].

Table 3.1. Measures of association for the 1996 Calabasas Fire.

Duration of 1996 Calabasas Simulation: 10/21 1100 to 10/21 2100 (10 hours)				<i>kappa</i>	<i>Jacard's</i>	<i>areal association</i>
FuelsUsed	Data Resolution	Weather Data	Fire Behavior Model	κ	C_J	C_A
cust	30m	che	HFIRE	0.1859	0.2051	0.6879
cust	30m	che	FARSITE	0.2066	0.2177	0.6938
cust	100m	che	HFIRE	0.2244	0.2226	0.7348
cust	100m	che	FARSITE	0.2271	0.2334	0.6804
cust	30m	mal	HFIRE	0.1838	0.2160	0.5774
cust	30m	mal	FARSITE	0.1763	0.2144	0.5364
cust	100m	mal	HFIRE	0.2328	0.2417	0.6419
cust	100m	mal	FARSITE	0.1779	0.2160	0.5292
nffl	30m	che	HFIRE	0.2963	0.3107	0.6332
nffl	30m	che	FARSITE	0.3331	0.3312	0.6745
nffl	100m	che	HFIRE	0.3284	0.3291	0.6646
nffl	100m	che	FARSITE	0.3145	0.3209	0.6516
nffl	30m	mal	HFIRE	0.3709	0.3554	0.7007
nffl	30m	mal	FARSITE	0.3265	0.3283	0.6618
nffl	100m	mal	HFIRE	0.3960	0.3685	0.7336
nffl	100m	mal	FARSITE	0.2069	0.2616	0.5345

The accuracy of both models was similar, but HFire was slightly more accurate than FARSITE in 6 of 8 trials as measured by C_A and 5 of 8 trials as measured by κ .

Using the HFire model, the average value of $C_J=0.28$ ($n=8$) and $C_A=0.67$ ($n=8$). For

FARSITE, the average value of $C_J=0.27$ ($n=8$) and $C_A=0.62$ ($n=8$). According to κ , the accuracy of all trials was greater than expected from chance with an average $\kappa=0.28$ ($n=8$) for HFire and an average $\kappa=0.25$ ($n=8$) for FARSITE. The trial with the best accuracy as measured by C_A , 0.7348, was achieved using the HFire model with the Cheesbro RAWS station weather data, custom fuels, and 100 meter spatial resolution. The predicted fire spread for this trial is shown in Figure 3.1. The trial with the best accuracy as measured by κ , 0.3960, was achieved using the HFire model with the Malibu RAWS weather station data, NFFL fuels, and 100 meter spatial resolution. The predicted fire spread for this trial is shown in Figure 3.4.

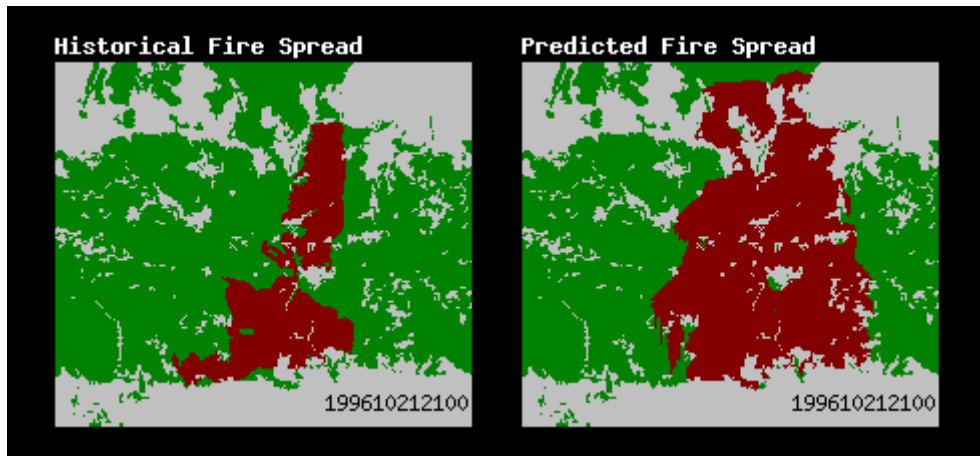


Figure 3.4. Historical (left) and predicted (right) fire behavior at 2100 hours during the 1996 Calabasas Fire using the HFire model. Example of high accuracy as measured by κ . Inputs used during this simulation: Malibu RAWS weather data, NFFL fuels, and 100 meter spatial resolution.

The trial with the least accuracy as measured by C_A , 0.5292, was achieved using the FARSITE model with the Malibu RAWS station weather data, custom fuels, and 100 meter spatial resolution. The predicted fire spread for this trial is shown in Figure 3.3. The trial with the least accuracy as measured by κ , 0.1763, was achieved using the FARSITE model with the Malibu RAWS weather station data, custom fuels, and 30 meter spatial resolution.

All of the Calabasas Fire simulations overpredicted the fire spread at the conclusion of the initial ten hour interval analyzed. In order to examine the accumulation of error on an hourly basis, a time series of cumulative predicted versus

historical area burned was constructed for the HFire and FARSITE simulations. Only simulations at 30 meter resolution are shown in order to limit the number of figures. Figure 3.5 depicts the cumulative area burned with simulations using custom fuels.

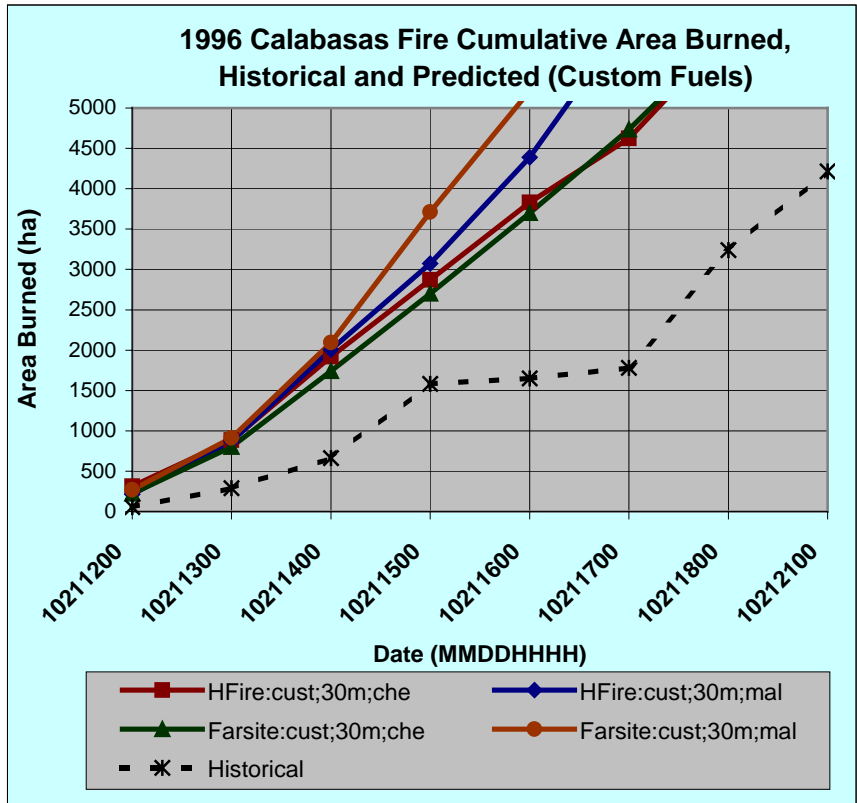


Figure 3.5. 1996 Calabasas Fire Cumulative Area Burned, Historical and Predicted (Custom Fuels). Results from HFire and FARSITE trials are shown. Simulation parameters are abbreviated as follows: cust, custom fuels; 30m and 100m, spatial data resolution; mal, Malibu RAWS; che, Cheesbro RAWS.

Figure 3.6 depicts the cumulative area burned with simulations using NFFL fuels.

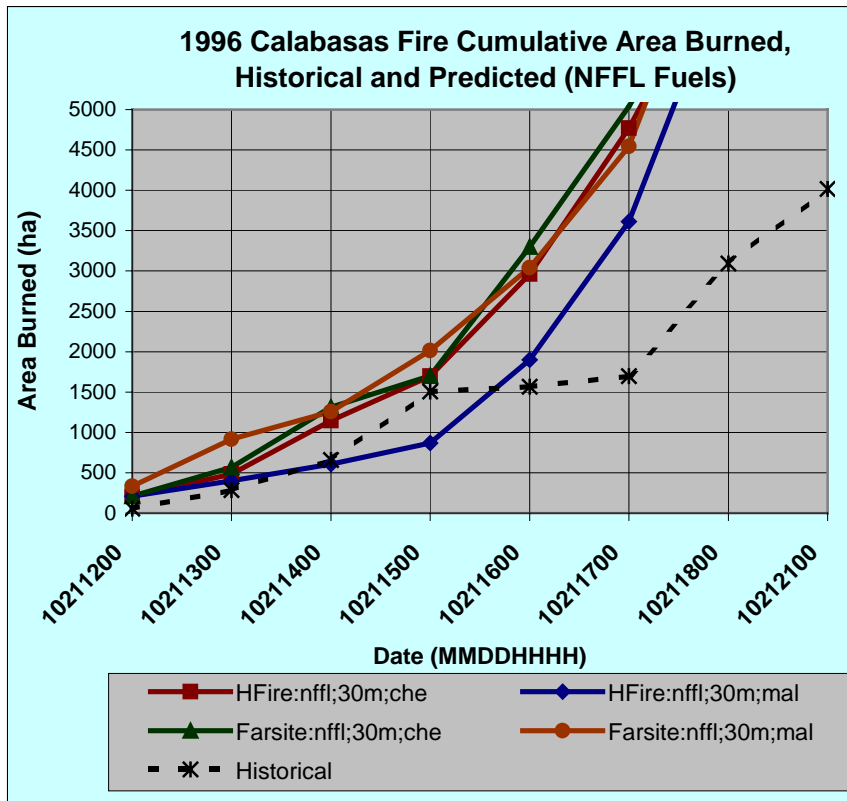


Figure 3.6. 1996 Calabasas Fire Cumulative Area Burned, Historical and Predicted (NFFL Fuels). Results from HFire and FARSITE trials are shown. Simulation parameters are abbreviated as follows: nffl, NFFL fuels; 30m and 100m, spatial data resolution; mal, Malibu RAWS; che, Cheesbro RAWS.

All of the simulations using custom fuels show rapid initial fire growth that did not occur in the historical data. Furthermore, the simulations using custom fuels were insensitive to the lull in fire spread that occurred in the historical data between 1500 and 1700 hours. In contrast, the simulations using the NFFL fuels matched the initial fire growth and thereafter accumulated error because they were also insensitive to the lull in historical fire spread. The lack of sensitivity on the part of both models from 1500 to 1700 hours could be due to a discrepancy in the windspeeds observed at the RAWS stations and the windspeed experienced at the fireline. Both the Cheesbro and Malibu RAWS stations show virtually no change in windspeed from 1400 to 1800 hours, with the exception of Cheesbro which shows a drop in windspeed at 1600 hours from 9.8 m/s (22 miles/hr) to 6.7 m/s (15 miles/hr). Suppression could also account for this lull in fire spread. Better agreement between observed and predicted

fire spread using the NFFL fuels could be explained by differences in the fuels within the area immediately surrounding the ignition point. In the NFFL fuels dataset, this area is assigned immature green brush (NFFL 5), whereas in the custom fuels this area is assigned the Santa Monica Mountains coastal sage scrub (custom 21).

3.2 1998 OGILVY FIRE

Unlike the Calabasas Fire, the 1998 Ogilvy Fire burned in the mountains of Ventura County, California under far more moderate weather conditions. The Ogilvy Fire actively spread for 161 hours, from the time of ignition on October 16 at 1500 hours until October 23 at 0800 hours. During this span, 1714 hectares, almost exclusively consisting of chaparral, were consumed by the fire. This represents less than half of the area consumed by the Calabasas Fire during the first 10 hours of spread. As a result, fire behavior during the Ogilvy Fire is representative of a more moderate fire event.

As in the case of the Calabasas fire, historical reference data collected via helicopter and GPS were available. However, the temporal resolution of the reference data was not as good, usually two estimates of the fire's location on any given day were available, one in the morning and one in the evening. In addition, the effect of suppression on the final fire spread perimeter was probably greater in the Ogilvy Fire because the less extreme fire behavior facilitated the use of multiple suppression techniques, such as hand crews and heavy equipment, to limit the fire's progress. This is a source of error when comparing predicted and observed fire behavior.

3.2.1 ASSEMBLING INPUT DATA

Historical windspeed and wind direction data during the fire were available on an hourly basis from one RAWS station, Los Prietos, located approximately 21 km

from the fire. Since the Los Prietos RAWS does not record dead fuel moisture, the Ojai RAWS station, located at 41 km from the fire, was used. Live fuel moisture during the simulation was held constant using values identical to those used for the Calabastas Fire, 50% ODW for live herbaceous material and 70% ODW for live woody material. Unlike dead fuel moisture, which varies diurnally, the variation in live fuel moisture is seasonal, with year-to-year differences being greatest at the start, rather than end, of the year. Because both fires occurred in late fall, it seems likely that the live fuel moisture of the shrubs during both fires were at a similar point in the phenological cycle.

NFFL and custom spatial fuels data reflecting 1998 conditions were produced using the same technique as was described for the Calabastas Fire, with two exceptions. First, no map of PNV existed for the area. Instead, a GAP Analysis vegetation map (Davis, et al., 1998) was used; vegetation type and PNV are not completely analogous. Second, new regrowth files were constructed for each GAP vegetation class. Although the custom fuels used in the Ogilvy Fire simulations included the wildland-urban interface fuel model, far less of the simulation domain consisted of wildland-urban interface areas in comparison to the Calabastas Fire.

Terrain elevation for the entire domain was available at the native resolution of the GAP vegetation map, 30 meters, so no resampling was required. An additional suite of 100 meter resolution spatial data inputs was generated using the same resampling techniques used for the Calabastas Fire.

3.2.2 ACCURACY OF PREDICTIONS

Four simulations of the Ogilvy Fire, representing all possible permutations of the fuels data sources and spatial data resolution, were performed for the HFire and FARSITE fire spread models. The full 161 hours of the fire were simulated with the intention of producing an accuracy assessment for the duration. Because some trials at the full duration completely consumed the simulation domain, a censored period of

time to assess accuracy was required. After examining the hourly output from each model, the first trial to completely consume the simulation domain required 89 hours. Thus, the predicted fire spread after 89 hours was used to compare to the historical reference data of fire spread after 89 hours.

The values of C_A , C_J , and κ , computed for all four simulations of the Ogilvy Fire using both the HFire and FARSITE models are shown in Table 3.2 [see Appendix G].

Table 3.2. Measures of association for the 1998 Ogilvy Fire.

Duration of 1998 Ogilvy Fire Simulation: 10/16 1500 to 10/20 0800 (89 hours)			<i>kappa</i>	<i>Jacard's</i>	<i>areal association</i>
FuelsUsed	Data Resolution	Fire Behavior Model	κ	C_J	C_A
cust	30m	HFIRE	0.0701	0.0564	0.6512
cust	30m	FARSITE	0.0371	0.0394	0.4908
cust	100m	HFIRE	0.1826	0.1192	0.8461
cust	100m	FARSITE	0.0368	0.0392	0.4884
nffl	30m	HFIRE	0.0019	0.0218	0.0636
nffl	30m	FARSITE	0.0001	0.0209	0.0228
nffl	100m	HFIRE	0.0043	0.0230	0.1129
nffl	100m	FARSITE	0.0000	0.0209	0.0209

Unlike the Calabasas Fire, in which the accuracy of both models was similar, the HFire model was measurably more accurate than FARSITE in all 4 trials as measured by C_A and κ . Using the HFire model, the average value for each measure of association was $C_J=0.06$ ($n=4$) and $C_A=0.42$ ($n=4$). For FARSITE, the average value of each measure of association was $C_J=0.03$ ($n=4$) and $C_A=0.26$ ($n=4$). According to κ , the accuracy of all trials using the FARSITE model was not greater than expected from chance. The only trials using the HFire model in which κ indicated the accuracy was better than expected from chance used the custom fuels. The trial with the best accuracy as measured by C_A , 0.8461, and κ , 0.1826, was achieved using the HFire model with the custom fuels and 100 meter spatial resolution. The historical and predicted fire spread for this trial is shown in Figure 3.7.



Figure 3.7. Historical (left) and predicted (right) fire behavior at 1700 hours on October 22 during the 1998 Ogilvy Fire using the HFire model. Example of severe overprediction. Inputs used during this simulation: custom fuels, and 100 meter spatial resolution.

The trial with the least accuracy as measured by C_A , 0.0209, and κ , 0.0000, was achieved using the FARSITE model with the NFFL fuels and 100 meter spatial resolution. Both trials using the FARSITE model and NFFL fuels completely consumed the simulation domain within the period analyzed.

All of the Ogilvy Fire simulations overpredicted fire spread in comparison to the historical data. In order to investigate the error further, a time series of cumulative area burned was constructed for the HFire and FARSITE simulations. From the results pictured in Figure 3.8, predictions of burned area in all simulation trials exceeded the area burned by the historical fire within 30 hours of the simulation onset. Only trials using custom fuel models are shown, because the overprediction error using NFFL fuels was considerably larger.

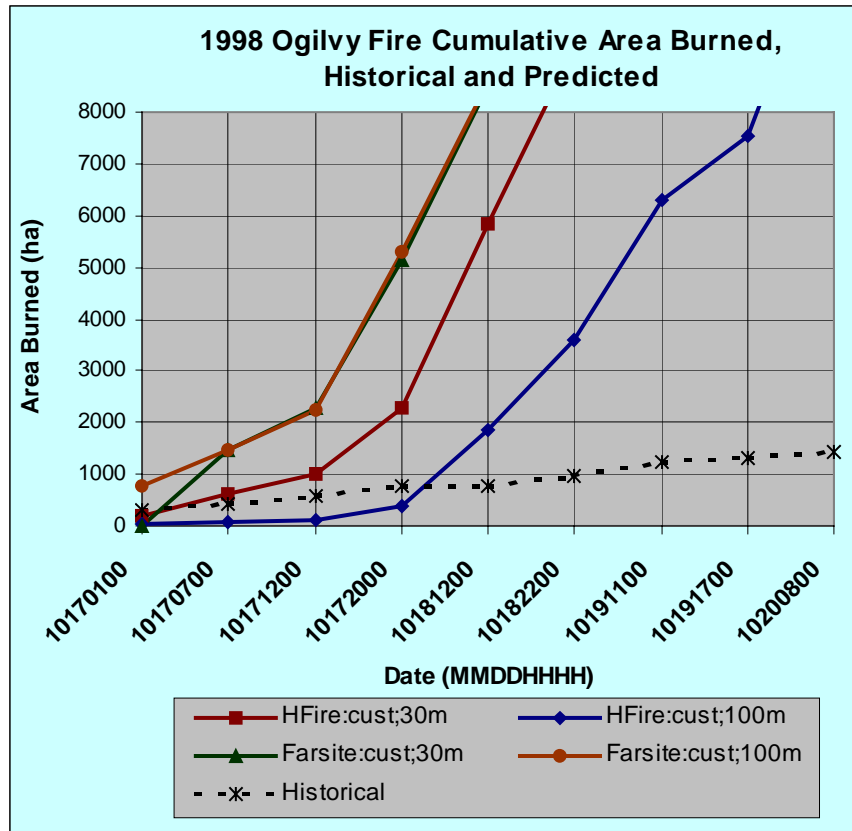


Figure 3.8. 1998 Ogilvy Fire Cumulative Area Burned, Historical and Predicted. Results from HFire and FARSITE trials are shown. Simulation parameters are abbreviated as follows: cust, custom fuels; 30m and 100m, spatial data resolution. FARSITE simulations at both spatial data resolutions, 30 and 100 meter, performed almost identically and show large error in predicted area within the first time period for which historical fire spread was available. Simulations using HFire exhibit the same general trend, however the trial using custom fuels at the 100 meter spatial resolution shows the best agreement with the historical data.

3.3 Results of Run Time Efficiency Tests

Table 3.3 shows the time, in seconds, required to simulate 10 hours of fire spread using the HFire model during the 1996 Calabasas Fire in Southern California. Each record in the table corresponds to one permutation of input variables. Individual simulation trials were repeated ten times for each suite of input data and the average

of the ten trials was assigned. The cumulative run time reflects the sum of the average of each suite of input data.

Table 3.3. Run time performance of HFire model during 1996 Calabasas Fire.

HFIRE Run Time Performance During 1996 Calabasas Simulation: 10/21 1100 to 10/21 2100 (10 hours)				<i>number of trials</i>	<i>average time to complete simulation</i>
Fuels Used	Data Resolution	Weather Data	Fire Behavior Model	n	secs
cust	30m	che	HFIRE	10	163.6
cust	100m	che	HFIRE	10	7.3
cust	30m	mal	HFIRE	10	204.5
cust	100m	mal	HFIRE	10	9.3
nffl	30m	che	HFIRE	10	180.8
nffl	100m	che	HFIRE	10	8.3
nffl	30m	mal	HFIRE	10	168.1
nffl	100m	mal	HFIRE	10	8.6
cumulative total					750.5
average (n=80)					93.8

An identical set of input data used during each trial with the HFire model, including terrain, fuels, and weather, was formatted for use with FARSITE. The only model parameter used in FARSITE without analogue in HFire was the specification of the distance and perimeter resolution of the simulation. Although all trials with FARSITE were first executed at the highest possible resolution of 60 and 30 meters respectively, in some cases this caused the simulator to enter an endless loop and become unresponsive. Values of distance and perimeter resolution were increased until this problem was resolved. Furthermore, the increased run time of each FARSITE trial precluded the replication of each trial as was done with the run time evaluation of HFire. Table 3.4 shows the run time performance of each trial using FARSITE.

Table 3.4. Run time performance of FARSITE model during 1996 Calabasas Fire.

FARSITE Run Time Performance During 1996 Calabasas Simulation: 10/21 1100 to 10/21 2100 (10 hours)				<i>perimeter resolution</i>	<i>distance resolution</i>	<i>time to complete simulation</i>
Fuels Used	Data Resolution	Weather Data	Fire Behavior Model	meters	meters	secs
cust	30m	che	FARSITE	60	30	7020
cust	100m	che	FARSITE	60	30	8220
cust	30m	mal	FARSITE	60	30	24840
cust	100m	mal	FARSITE	120	60	3480
nffl	30m	che	FARSITE	120	60	7740
nffl	100m	che	FARSITE	300	150	300
nffl	30m	mal	FARSITE	120	60	16080
nffl	100m	mal	FARSITE	300	150	1320
cumulative total						69000
average (n=8)						8625

As with all raster models, the performance of the HFire model is proportional to the number of cells in the simulation domain due to the repeated scans through the domain performed by the model. In contrast, FARSITE model performance is a function of the user-specified simulation resolution and the relative heterogeneity of the conditions of fire spread; FARSITE adaptively increases the density of vertices when the conditions of fire spread change. The cumulative run time of all eight FARSITE trials, 69,000 seconds, was 92 times larger than the cumulative run time of the average of all eight HFire trials, 750 seconds.

4.0 CONCLUSIONS

A description and accuracy assessment of the HFire model, a new raster-based spatially explicit model of surface fire spread through chaparral, was presented. HFire is an improvement on existing raster models of fire spread for several reasons. First, the adaptive timestep strategy is an elegant alternative to fixed interval models because the simulation clock responds to the fire behavior and increments more slowly during periods of rapid fire spread and more rapidly under moderate fire spread. Although event-driven simulations, such as a cell contact model, offer a similarly elegant solution with respect to simulation clock management, these models suffer by forcing fire spread to occur in unit distances equal to the cell size. Therefore, the second major advance of the HFire model is to allow fire spread to occur in distance increments smaller than the cell size using the technique of finite fractional distances. Managing fire spread in finite distances between cells allows the effect of a fire spreading into a cell from alternating directions to be captured, as well as fire spread that results from prior heating during previous iterations in the simulation. The cumulative benefit of both of these features is to reduce distortion of fire spread typically produced with other raster models.

The sensitivity of the HFire model to input fuels data varied based upon the severity of conditions forcing fire spread. Simulations of the 1996 Calabasas Fire, which spread under extreme conditions, showed a small difference in accuracy using the two fuels data sources, average $C_A=0.66$ ($n=4$) for custom fuels and average $C_A=0.68$ ($n=4$) for NFFL fuels. This observation is consistent with Bossert et al. (2000) who found similar conclusions during a comparison using a coupled atmosphere and fire model to simulate a very small subset of the Calabasas Fire. Under moderate fire spread conditions during the 1998 Ogilvy Fire, the simulation accuracy showed pronounced sensitivity to input fuels, average $C_A=0.75$ ($n=2$) for custom fuels and average $C_A=0.09$ ($n=2$) for NFFL fuels. These results indicate that high quality fuels information is most beneficial to fire management personnel for use

in predicting fire behavior during prescribed fires or early season burns. During wind-driven wildland fires, the quality of the fuels information is less influential.

In comparison to the results found for fuels, the sensitivity of the HFire model to input spatial data resolution was weaker. In both the Calabasas and Ogilvy Fire simulations, the average accuracy as measured by C_A was slightly larger for the trials using 100 meter resolution data. This effect was most pronounced in the Ogilvy Fire simulation using custom fuels. The C_A at 30 meter resolution, 0.65, was not nearly as good as the C_A at 100 meter resolution, 0.85. The reason for this somewhat counterintuitive result is most likely due to the extinction mechanism used in HFire. Since the same extinction coefficient was used for all trials and extinction operates by extinguishing fires unable to spread out of a cell, this mechanism is coupled to the spatial data resolution. This explains the reason for the improved accuracy, shown in Figure 3.6, using HFire during the Ogilvy Fire with custom fuels at 100 meter resolution in comparison to 30 meter resolution. Future simulations should differentiate the extinction coefficient used based upon the cell size of the input spatial data.

The run time efficiency gains using the HFire model are an especially valuable feature of an operational model for several reasons. First, predictions from multiple alternative scenarios, perhaps reflecting best and worst cases, can be performed with HFire in the same amount of time required for FARSITE to generate a single prediction. Two, the impact of changing conditions on predictions, perhaps based on revised weather forecasts, can be more quickly relayed to fire management using HFire. Three, the HFire model performs fast enough to allow spatial fire prediction capabilities to be made available to personnel distributed at disparate locations using a web browser or wireless device.

Based on accuracy and run time efficiency comparisons to the FARSITE model during historical simulations, HFire offers several advantages as an operational model of fire spread through chaparral. First, HFire executes more quickly than FARSITE. The Calabasas Fire spread under extreme conditions through complex and

dissected terrain, and both models produced patterns of fire spread with statistically similar accuracy, average $C_A=0.67$ ($n=4$) for HFire and average $C_A=0.62$ ($n=4$) for FARSITE. However, the HFire model simulation executed all experimental trials orders of magnitude faster than the vector code used by FARSITE. Previous researchers have identified the difficulty that models implemented using Huygens' Principle, such as FARSITE, have in heterogeneous conditions. Although heterogeneity is a relative term, the drastic reduction in run time performance of the FARSITE model during the simulations of extreme fire behavior is a clear indication that the vector code is not well suited to predicting fire behavior under these conditions. The HFire model may represent an alternative management tool to use during complex fire situations. The second advantage of the HFire model is the extinction feature, which extinguishes a cell when the fire behavior is insufficient for propagating into an adjacent cell. In comparison to the vector code, the incorporation of fire extinction in HFire resulted in measurably superior accuracy for the historical simulation of moderate fire spread. The average of all HFire trials during the Ogilvy Fire $C_A=0.42$ ($n=2$) was well above the average of all trials for FARSITE $C_A=0.26$ ($n=2$). In fire spreading through chaparral areas under moderate conditions, fire management personnel will often apply a rate of spread reduction factor within FARSITE to control the overprediction error. Since no rate of spread adjustments were applied during this analysis, the data presented here confirms that FARSITE quickly overpredicts fire spread in this situation. Unlike rate of spread reduction factors, the coefficient used to control extinction in HFire is based upon physical reasoning and is activated by the fire behavior itself. Furthermore, even though extinction was enabled for both extreme and moderate simulations, this feature only had an effect whenever and wherever the fire behavior dictated.

4.1 FUTURE WORK

Several areas of future work exist. First, new methods for assessing the accuracy of spatially explicit models of fire spread are needed. Although the measures of association presented here provide some indication of the accuracy of a particular model, none implicitly contain a spatial component. For example, a useful spatial metric of accuracy would be able to indicate that the bulk of the overprediction error was occurring along the flanks of the fire rather than at the head portions of the fire. This would verify whether the fire spread equations or method used to apply those equations to two-dimensions are the source of error. A preliminary attempt was made to do this with the data generated from the Calabasas Fire, but without interesting conclusions. Second, the accuracy assessment presented here was limited to the final spread of the fire only. Additional information could be gained by exploring the change in the accuracy on an hour-by-hour basis. Any temporal patterns that exist in the error could ultimately lead to future work which applies a self-correction mechanism to the fire spread model to minimize this error. Third, accuracy assessment of the HFire and FARSITE models using additional fires is required to confirm some of the conclusions presented here. Fourth, replacing some of the empirical terms in the Rothermel spread equation with physically based expressions could provide a more versatile model of fire spread in chaparral, particularly with respect to the interaction between wind and slope on the fire.

REFERENCES CITED

- Albini, FA and RG Baughman. 1979 Estimating windspeeds for predicting wildland fire behavior. USDA Forest Service, Intermountain Forest and Range Experiment Station. Research Paper, INT-221. Ogden, UT. 12p.
- Albini, FA, and CH Chase. 1980. Fire Containment Equations For Pocket Calculators. USDA Forest Service, Intermountain Forest and Range Experiment Station. Research Note, INT-268. Ogden, UT. 17p.
- Anderson, HE. 1982. Aids to Determining Fuel Models For Estimating Fire Behavior. USDA Forest Service, Intermountain Forest and Range Experiment Station. General Technical Report, INT-122. Ogden, UT. 22 p.
- Anderson, HE. 1983. Predicting wind-driven wildland fire size and shape. USDA Forest Service, Intermountain Forest and Range Experiment Station. Research Paper, INT-305. Ogden, Utah. 26p.
- Andrews, PL. 1986. BEHAVE: Fire Behavior Prediction and Fuel Modeling Subsystem- BURN Subsystem, Part 1. USDA Forest Service, Intermountain Forest and Range Experiment Station. General Technical Report, INT-194. Ogden, UT. 130p.
- Beer, T. 1990. The Interaction of Wind and Fire. *Boundary Layer Meteorology*. 54. 287-308.
- Bossert, JE, RR Linn, JM Reisner, JL Winterkamp, P Dennison, and DA Roberts. 2000. Coupled Atmosphere-Fire Behavior Model Sensitivity to Spatial Fuels Characterization. Preprint, Third Symposium on Fire and Forest Meteorology, Amer. Meteor. Soc. 80th Annual Meeting, Long Beach, CA, 9-14 January, 2000. pp. 21-26.
- Bratley, P, BL Fox, and LE Schrage. 1987. *A Guide to Simulation*. Springer-Verlag. New York. 397p.
- Catchpole, T and N DeMestre. 1986. Physical models for a spreading line fire. *Australian Forestry*. 49(2). 102-111.
- Catchpole, EA, WR Catchpole, and RC Rothermel, 1993. Fire Behavior Experiments in Mixed Fuel Complexes. *International Journal of Wildland Fire*. 3(1). 45-57.
- Catchpole, WR, EA Catchpole, BW Butler, RC Rothermel, GA Morris, and DJ Latham. 1998. Rate of Spread of Free-Burning Fires in Woody Fuels in a Wind Tunnel. *Combustion Science and Technology*. 131. 1-37.

Clarke, KC, JA Brass, and PJ Riggan. 1994. A Cellular Automaton Model of Wildfire Propagation and Extinction. *Photogrammetric Engineering and Remote Sensing*. 60(11): 1355 - 1367.

Cohen, J. 1960. A Coefficient of Agreement for Nominal Scales. *Educational and Psychological Measurement*. 20. 37 -46.

Conard, SG and DR Weise. 1998. Management of fire regime, fuels, and fire effects in southern California chaparral: lessons from the past and thoughts for the future. *Proc. 20th Tall Timbers Fire Ecology Conference*. 342-350.

Davis, F W, DM Stoms, AD Hollander, KA Thomas, PA Stine, D Odion, MI Borchert, JH Thorne, MV Gray, RE Walker, K Warner, and J Graae. 1998. *The California Gap Analysis Project – Final Report*. University of California, Santa Barbara. 255 pp.

Finney, MA. 1998. *FARSITE: Fire Area Simulator- Model Development and Evaluation*. USDA Forest Service, Rocky Mountain Research Station. Research Paper, RMRS-RP-4. 47p.

Fons, WL. 1946. Analysis of fire spread in light fuels. *Journal of Agricultural Research*. 72(3): 93-121.

Fosberg, MA. 1977. *Forecasting the 10-Hour Timelag Fuel Moisture*. USDA Forest Service. Research Paper, RM-187. 10p.

Frandsen, WH. 1971. Fire Spread through Porous Fuels from the Conservation of Energy. *Combustion and Flame*. 16. 9-16.

Frandsen, WH. 1973. *Effective heating of fuel ahead of spreading fire*. USDA Forest Service Research Paper INT-140. 16p.

Frandsen, WH and PL Andrews. 1979. *Fire behavior in nonuniform fuels*. USDA Forest Service, Intermountain Forest and Range Experiment Station. Research Paper, INT-232. Ogden, UT. 34p.

Franklin, J. 1997. *Forest Service Southern California Mapping Project: Santa Monica Mountains National Recreation Area, Final Report*. Unpublished report. 11p.

French, IA, DH Anderson, and EA Catchpole. 1990. *Graphical Simulation of Bushfire Spread*. *Mathematical Computer Modelling*. 13(12): 67-71.

- Fujioka, F. 1985. Estimating wildland fire rate of spread in a spatially nonuniform environment. *Forest Science*. 31(1). 21-29.
- Green, DG. 1983. Shapes of Simulated Fires in Discrete Fuels. *Ecological Modelling*. 20. 21-32.
- Green, DG, A Tridgell, and MA Gill. 1990. Interactive Simulation of Bushfires in Heterogeneous Fuels. *Mathematical Computer Modelling*. 13(12): 57-66.
- Keeley, JE, CJ Fotheringham, and M Morais. 1999. Reexamining Fire Suppression Impacts on Brushland Fire Regimes. *Science*. 284. 1829-1832.
- Kourtz, PH, and WG O'Regan. 1971. A model for a small forest fire, to simulate burned and burning areas for use in a detection model. *Forest Science*. 17. 163-169.
- McAlpine, RS and BM Wotton. 1993. The use of Fractal Dimension to Improve Wildland Fire Perimeter Predictions. *Canadian Journal of Forest Research*. 23. 1073-1077.
- Moritz, MA. 1997. Analyzing Extreme Disturbance Events: Fire in Los Padres National Forest. *Ecological Applications*. 7(4). 1252-1262.
- Pitts, WM. 1991. Wind effects on fires. *Progress Energy Combustion Science*. 17:83-134.
- Richards, GD. 1988. Numerical Simulation of Forest Fires. *International Journal for Numerical Methods in Engineering*. 25. 625-633.
- Richards, GD. 1990. An Elliptical Growth Model Of Forest Fire Fronts And Its Numerical Solution. *International Journal for Numerical Methods in Engineering*. 30. 1163-1179.
- Riggan, PJ, S Goode, PM Jacks, and RN Lockwood. 1988. Interaction of Fire and Community Development in Chaparral of Southern California. *Ecological Monographs*. 58(3). 155-176.
- Roberts, DA, M Gardner, R Church, S Ustin, G Scheer, RO Green. 1998. Mapping Chaparral in the Santa Monica Mountains Using Multiple Endmember Spectral Mixture Models. *Remote Sensing of Environment*. 65. 267-279.
- Roberts, DA, PE Dennison, M Morais, ME Gardner, J Regelbrugge, and SL Ustin. 1999. Mapping Wildfire Fuels using Imaging Spectrometry along the Wildland Urban Interface. *Proc. of the Joint Fire Science Conference and Workshop, June 17-19, 1999, Boise, Idaho, Vol. 1, 212-223.*

Rothermel, RC. 1972. A Mathematical Model for Predicting Fire Spread in Wildland Fuels. USDA Forest Service, Intermountain Forest and Range Experiment Station. Research Paper, INT-115. Ogden, UT. 40p.

Rothermel, RC and Philpot, CW. 1973. Predicting changes in chaparral flammability. *Journal of Forestry*. 71(1):640-643.

Rothermel, RC. 1983. How to predict the spread and intensity of forest and range fires. USDA Forest Service, Intermountain Forest and Range Experiment Station. General Technical Report, INT-143. Ogden, UT. 161p.

Rothermel, RC, RA Wilson, GA Morris, SS Sackett. 1986. Modeling Moisture Content of Fine Dead Wildland Fuels: Input to the BEHAVE Fire Prediction System. USDA Forest Service, Intermountain Forest and Range Experiment Station. Research Paper, INT-359. Ogden, UT. 61p.

Rothermel, RC. 1991. Predicting Behavior and Size of Crown Fires in the Northern Rocky Mountains. USDA Forest Service, Intermountain Forest and Range Experiment Station. Research Paper, INT-438. Ogden, UT. 46p.

Serrano, L, SL Ustin, DA Roberts, JA Gamon, and J Penuelas. 2000. Deriving Water Content of Chaparral Vegetation from AVIRIS Data. *Remote Sensing of Environment*. 74. 570-581.

Stevenson, AE, DA Schermerhorn, and SC Miller. 1974. Simulation of Southern California Forest Fires. In 15th Symposium (International) on Combustion. The Combustion Institute. Pittsburgh, PA. 147-155.

Ustin, SL, DA Roberts, J Pinzon, S Jacquemoud, M Gardner, G Scheer, CM Castaneda, and A Palacios-Orueta. 1998. Estimating canopy water content of chaparral shrubs using optical methods. *Remote Sensing of Environment*. 65. 280-291.

VanWilgen, BW, DC Le Maitre, and FJ Kruger. 1985. Fire modelling in South African fynbos (macchia) vegetation and predictions from Rothermel's fire model. *Journal of Applied Ecology*. 22. 207-216.

Weber, RO. 1991. Modeling fire spread through fuel beds. *Progress Energy Combustion Science*. 17:67-82.

Weise, DR, and GS Biging. 1997. A Qualitative Comparison of Fire Spread Models Incorporating Wind and Slope Effects. *Forest Science*. 43(2):170-180.

Weise, DR, and JC Regelbrugge. 1997. Recent chaparral fuel modeling efforts, submitted to California Fuels Committee Newsletter. Prescribed Fire and Fire Effects Research Unit, Riverside Fire Laboratory, Pacific Southwest Research Station. 3p.

Weise, DR, and FM Fujioka. 1998. Comparison of Fire Spread Estimates Using Weather Station Observations Versus Nested Spectral Model Gridded Weather. In 2nd Symposium on Fire and Forest Meteorology. 11-16 January. Phoenix, AZ. American Meteorological Society. 75-79.

Williams, FA. 1976. Mechanisms of Fire Spread. In 16th Symposium (International) on Combustion. The Combustion Institute. Pittsburgh, PA. 1281-1294.

Wilson, RA. 1990. Reexamination of Rothermel's Fire Spread equations in No-Wind and No-Slope Conditions. USDA Forest Service, Intermountain Forest and Range Experiment Station. Research Paper, INT-434. Ogden, UT. 13p.

Zack, JA and RA Minnich. 1991. Integration of Geographic Information Systems with a Diagnostic Wind Field Model for Fire Management. Forest Science. 37(2). 560-573.

APPENDIX A: FUEL MODEL DESCRIPTION FILE

Table A.1 lists the attributes, in metric units, supplied for each fuel model inside the fuel model description (.fmd) file. Table A.2 lists descriptions of the abbreviated field names used in Table A.1. Table E.1 lists a short descriptive name and reference for each fuel model number in Table A.1.

Table A.1. Fuel model properties listed in fuel model description file.

Model	D1H	D10H	D100	LH	LW	D1HSAV	LHSAV	LWSAV	FDEPTH	MEX	DHC	LHC
Units	Mg/ha	Mg/ha	Mg/ha	Mg/ha	Mg/ha	1/cm	1/cm	1/cm	cm	%	kJ/kg	kJ/kg
1	1.66	0.00	0.00	0.00	0.00	105.98	0.00	0.00	30.48	12	18608	18608
3	6.75	0.00	0.00	0.00	0.00	45.42	0.00	0.00	76.20	25	18608	18608
4	11.23	8.99	4.51	0.00	11.21	60.56	0.00	45.42	182.88	20	18608	18608
5	2.24	1.12	0.00	0.00	4.48	60.56	0.00	45.42	60.96	20	18608	18608
6	3.36	5.60	4.48	0.00	0.00	52.99	0.00	0.00	76.20	25	18608	18608
7	2.53	4.19	3.36	0.00	0.83	52.99	0.00	46.93	76.20	40	18608	18608
9	6.55	0.92	0.34	0.00	0.00	75.70	0.00	0.00	6.10	25	18608	18608
15	4.48	6.73	2.24	1.12	4.48	19.37	66.61	19.37	91.44	13	23260	23260
16	5.04	10.76	4.04	6.73	6.28	15.14	45.42	15.14	182.88	15	18608	18608
17	2.91	2.24	2.24	4.48	4.48	19.37	66.61	19.37	121.92	20	18608	18608
18	12.33	1.79	0.22	1.68	5.60	19.37	45.42	19.37	91.44	25	21399	21399
20	1.66	4.19	3.36	0.00	0.83	105.98	45.42	46.93	53.34	40	18608	18608
21	5.50	0.70	0.00	1.60	3.00	19.37	45.42	19.37	91.44	25	21399	21399

Table A.2. Fields used in fuel model description file.

Model	Fuel Model Number
D1H	Accumulated Dead 1 Hour Fuels
D10H	Accumulated Dead 10 Hour Fuels
D100H	Accumulated Dead 100 Hour Fuels
LH	Accumulated Live Herbaceous Fuels
LW	Accumulated Live Woody Fuels
D1HSAV	Dead 1 Hour Fuels Surface Area to Volume (SAV) Ratio
LHSAV	Live Herbaceous Fuels Surface Area to Volume (SAV) Ratio
LWSAV	Live Woody Fuels Surface Area to Volume (SAV) Ratio
FDEPTH	Fuel Bed Depth (70% of Average Stand Height)
MEX	Moisture of Extinction of Dead Fuels
DHC	Dead Fuels Heat Content
LHC	Live Fuels Heat Content

APPENDIX B: FUEL PARTICLE SIZE CLASSES AND FIRE BEHAVIOR

Since the fuel particle diameter is strongly correlated to the SAV ratio and diameter is an easier quantity to measure empirically, field fuel inventory data is often collected and summarized by fuel particle diameter rather than SAV. The stem diameter size classes, also referred to as Equilibrium Moisture Content (EMC) Timelag classes, into which the physical properties of the fuel bed are organized is shown in Table B.1. According to Fosberg (1977), Byram defined the timelag as the “time interval required for the fuel moisture to change $1-1/e$ (or approximately $2/3$) of the difference between a uniform starting equilibrium value to a new uniform equilibrium after the environment was changed instantly”. Although EMC is typically used to describe the diameter of dead fuels only, the diameter of live fuels are sometimes referred to by EMC size class as well, despite the fact that their behavior with respect to fuel moisture is understood to be different from dead fuels.

Table B.1. Relationship between EMC size classes and fuel particle diameter.

Fuel Particle Equilibrium Moisture Content (EMC) Timelag Class Name	Fuel Particle Stem Diameter Size
1 Hour EMC Timelag	< 0.635 cm
10 Hour EMC Timelag	0.635 cm to 2.54 cm
100 Hour EMC Timelag	2.54 cm to 7.62 cm
1000 Hour EMC Timelag	> 7.62 cm

If we assume that all of the fuel particles in a fuel bed are approximately cylindrical in shape, then the stem diameter of a fuel particle can be related to its SAV. In general, larger diameter cylinders have lower values of SAV, diminishing the exposed fuel particle surface which can take part in the chemical reactions of combustion.

Table B.2. Relationship between stem diameter and surface area to volume ratio.

Fuel Particle Stem Diameter Size Class	Units	Surface-Area-to-Volume (SAV) Ratio	Reference
0 - 0.5 cm	m ² /m ³	2400	Riggan, et al 1988
0.5 - 1.0 cm	m ² /m ³	535	Riggan, et al 1988
1.0 - 2.0 cm	m ² /m ³	265	Riggan, et al 1988
> 2.0 cm	m ² /m ³	90	Riggan, et al 1988
Sclerophytic <i>Ceanothus</i> Foliage	m ² /m ³	3100	Riggan, et al 1988
Mesophytic <i>Ceanothus</i> Foliage	m ² /m ³	6900	Riggan, et al 1988
<i>Adenostoma fasciculatum</i> Needles	m ² /m ³	6662	Rothermel and Philpot, 1973

Using limited empirical evidence, Frandsen (1973) was able to construct an approximate relationship between the SAV ratio of a fuel particle and the fraction of the mass of that particle that was brought to ignition, Equation (B.1).

$$\varepsilon = e^{-\left(\frac{1}{0.0022s_{fp}}\right)} \quad (\text{B.1})$$

The fraction of the fuel mass heated to ignition, ε , is assumed to be equivalent to the outermost 0.0022m of the fuel particle with a given SAV ratio, s_{fp} . Figure B.1 shows the curve of this relationship across a continuum of SAV ratios. Although both high and low SAV fuels may burn during a fire, the distinction between the two is important because the high SAV fuels burn first. The time required to bring the high SAV fuels to ignition, also known as the residence time, governs the rate of fire spread. Consequently, fuels characterized by a high SAV ratio, such as grass, exhibit rapid rates of spread because the fire residence time is relatively short.

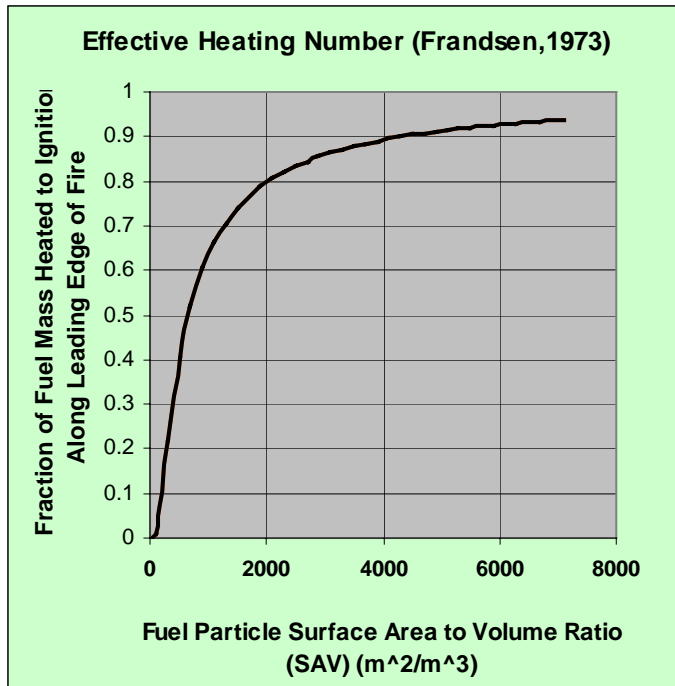


Figure B.1. Frandsen's Effective Heating Number.

As an example of applying the relationship presented in Figure B.1 to the SAV values from Table B.2, one can infer that nearly all of the mass (> 0.85%) of the foliage in chaparral shrubs, with SAV generally in excess of 3000 m²/m³, will contribute to the forward rate of spread of the fire.

APPENDIX C: WINDSPEED REDUCTION

The relationship presented by Albini and Baughman (1979) enables measurements of the windspeed at a reference height above the fuel bed to be related to the windspeed at midflame which drives fire behavior. Figure C.1 shows the effect of this relationship for four values of windspeed measured at reference height, $U_{ref} = \{2.5\text{m/s}; 5.0\text{ m/s}; 7.5\text{ m/s}; 10.0\text{ m/s}\}$. For example, a windspeed of 7.5 m/s at reference height will be reduced to approximately 2.0 m/s at 1.0 m above the ground and approximately 3.0m/s at 5 m above the ground. The effect on fire behavior of a reduction in windspeed of this magnitude will be pronounced. Since the reference height is always measured from the top of the fuel bed, the values in the figure begin to asymptote above 6.096 m.

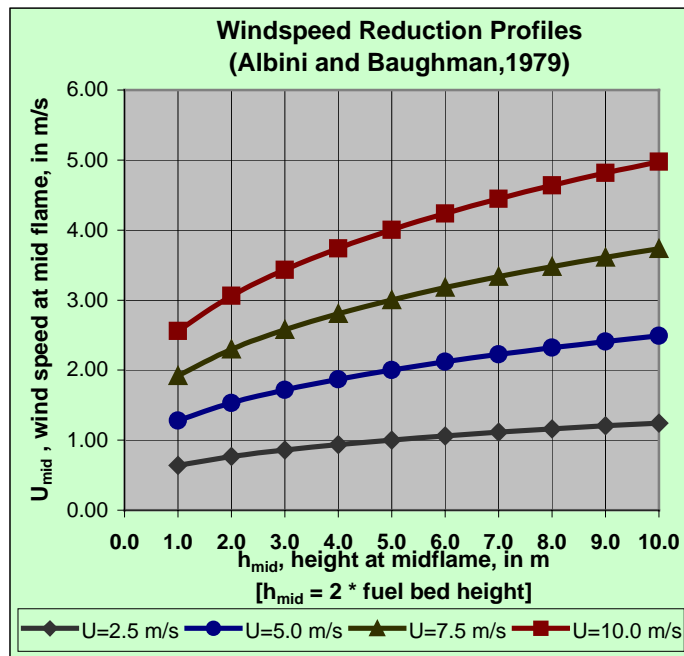


Figure C.1. Windspeed reduction profile of various windspeeds recorded at reference height ($h_{ref} = 6.096\text{ m}$ above the fuel bed for all cases).

APPENDIX D: ESTIMATING FIRE SPREAD AT ARBITRARY DIRECTIONS

The solution to the fire containment problem (Albini and Chase, 1980) provides the rate of fire spread at an arbitrary direction using two pieces of information: the fire's maximum rate of spread and length to width ratio, Equations (2.4) and (2.5). Figure D.1 shows the rate of fire spread as a fraction of maximum for a range of length to width ratios, $L/W = \{6.0; 4.0; 2.0; 1.0\}$, and at angles increasing in severity from 0.0 (R_{max}) to 180.0. The length to width ratios used represent a general bound on the values observed from fire shapes in the field (Anderson, 1983). Since the relationship is symmetrical about 0.0, other azimuths are not shown. In the case of a fire spreading with a length to width ratio of 1.0, a perfect circle, the property of Equation (2.4) ensures that the rate of spread in all directions is equal. As the length to width ratio of the fire increases, the more dramatic the reduction in the rate of fire spread in directions off maximum.

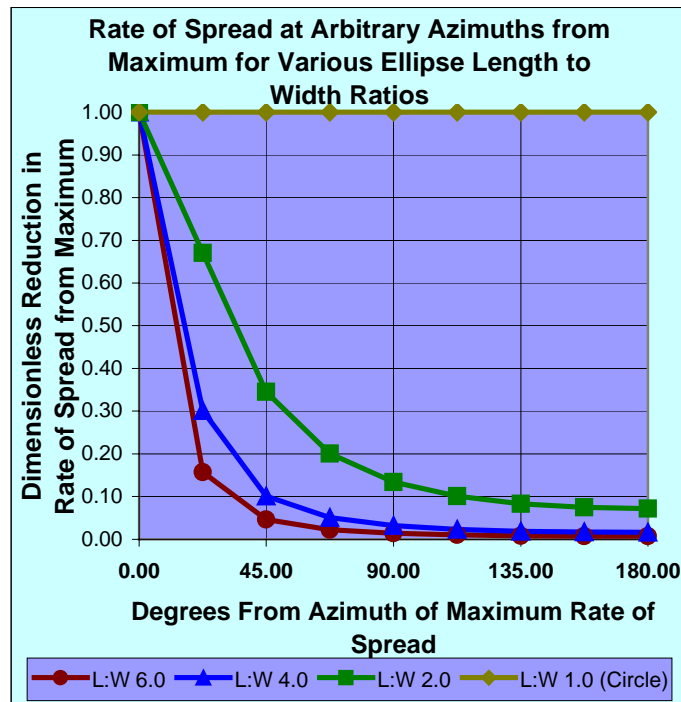


Figure D.1. Rate of fire spread at arbitrary directions as a fraction of maximum and function of length to width ratio.

APPENDIX E: REGROWTH FILE USED TO GENERATE FUELS MAPS

On the following page, Table E.2 shows a portion of the successional pathway table, truncated to 20 years, contained in the regrowth file that was used to generate a custom fuels map for the Santa Monica Mountains. The table indexes potential natural vegetation (PNV) types to the fuel models most representative of the regrowth sequence of that PNV. The PNV name is located in the first column for convenience, followed by a numerical index. The remaining columns contain an array of fuel model numbers to assign to the PNV at a particular year postfire. The fuel model numbers used in the file are listed along with a short descriptive name in Table E.1. For example, a cell with a PNV of chamise chaparral (PNV=6) will be assigned the ‘young Chamise’ fuel model (fuel model=17) during 3 to 15 years postfire, and the ‘old Chamise’ fuel model (fuel model=15) thereafter. A program which reads raster format (ASCII or binary) PNV and stand age spatial data along with a regrowth file of the format shown in Table E.2 handles the construction of the output fuels raster file used by the simulation. This program is also incorporated into the HFire code as a potential step during simulation preprocessing.

Table E.1. Fuel model numbers and description.

Fuel Model Number	Description	Source	Reference
1	short grass	NFFL	Anderson, 1982
3	tall grass	NFFL	Anderson, 1982
4	chaparral	NFFL	Anderson, 1982
5	brush	NFFL	Anderson, 1982
6	dormant brush	NFFL	Anderson, 1982
7	southern rough	NFFL	Anderson, 1982
9	hardwood litter/riparian	NFFL	Anderson, 1982
15	old Chamise	USFS	Weise and Regelbrugge, 1997
16	Ceanothus	USFS	Weise and Regelbrugge, 1997
17	young Chamise	USFS	Weise and Regelbrugge, 1997
18	sagebrush and buckwheat	USFS	Weise and Regelbrugge, 1997
20	wildland urban interface	UCSB	unpublished
21	SMM coastal sage scrub	UCSB	unpublished
98	water	unburnable	
99	rock/agriculture	unburnable	

Table E.2. Successional pathways table used to index PNV type and stand age to a custom fuel model number in the Santa Monica Mountains. The ‘PNV Description’ column is not included in the regrowth file supplied for processing.

PNV DESCRIPTION	PNV	y1	y2	y3	y4	y5	y6	y7	y8	y9	y10	y11	y12	y13	y14	y15	y16	y17	y18	y19	y20
unburnable	0	99	99	99	99	99	99	99	99	99	99	99	99	99	99	99	99	99	99	99	99
coastal dune/bluff scrub	1	99	99	99	99	99	99	99	99	99	99	99	99	99	99	99	99	99	99	99	99
coastal sage scrub	2	1	1	1	21	21	21	21	21	21	21	21	21	21	21	21	18	18	18	18	18
coastal sage scrub-chaparral transition	3	1	1	1	21	21	21	21	21	21	21	21	21	16	16	16	16	16	16	16	16
northern mixed chaparral	4	1	1	18	18	18	18	18	18	18	18	18	18	16	16	16	16	16	16	16	16
red shank chaparral	5	1	1	17	17	17	17	17	17	17	17	17	17	17	17	17	15	15	15	15	15
chamise chaparral	6	1	1	17	17	17	17	17	17	17	17	17	17	17	17	17	15	15	15	15	15
coastal cactus scrub	7	1	1	1	1	1	1	1	1	1	1	1	1	1	1	1	1	1	1	1	1
non-native grassland/herbaceous	8	1	1	1	1	1	1	1	1	1	1	1	1	1	1	1	1	1	1	1	1
rock outcrops (barren inland)	9	99	99	99	99	99	99	99	99	99	99	99	99	99	99	99	99	99	99	99	99
salt marsh	10	99	99	99	99	99	99	99	99	99	99	99	99	99	99	99	99	99	99	99	99
valley oak	11	1	1	1	1	1	1	1	1	1	1	1	1	1	1	1	1	1	1	1	1
coast live oak	12	3	3	3	3	3	3	3	3	3	3	3	3	3	3	3	3	3	3	3	3
walnut	13	1	1	1	1	1	1	1	1	1	1	1	1	1	1	1	1	1	1	1	1
riparian (Sycamore-Oak)	14	9	9	9	9	9	9	9	9	9	9	9	9	9	9	9	9	9	9	9	9
non-native conifer/hardwood	15	9	9	9	9	9	9	9	9	9	9	9	9	9	9	9	9	9	9	9	9
coastal strand	16	99	99	99	99	99	99	99	99	99	99	99	99	99	99	99	99	99	99	99	99
water	17	98	98	98	98	98	98	98	98	98	98	98	98	98	98	98	98	98	98	98	98
development	18	20	20	20	20	20	20	20	20	20	20	20	20	20	20	20	20	20	20	20	20
agriculture	19	99	99	99	99	99	99	99	99	99	99	99	99	99	99	99	99	99	99	99	99
NPS riparian vegetation	99	9	9	9	9	9	9	9	9	9	9	9	9	9	9	9	9	9	9	9	9
NO DATA	255	99	99	99	99	99	99	99	99	99	99	99	99	99	99	99	99	99	99	99	99

APPENDIX F: 1996 CALABASAS FIRE SIMULATION: RAW RESULTS

Table F.1 shows the area totals at the conclusion of 10 hours of the 1996 Calabasas Fire. These totals were used to generate the measures of association used to evaluate the accuracy of the HFire and FARSITE models. Although not reported in the main body of the text, additional measures of association other than C_J , C_A , and κ were calculated using the data in Table F.1. The values of the additional coefficients appear in Table F.2.

Table F.1. Correspondence Table For Observed and Predicted Fire Spread During the 1996 Calabasas Fire

Duration of 1996 Calabasas Simulation: 10/21 1100 to 10/21 2100 (10 hours)				ha	ha	ha	ha	ha	ha
FuelsUsed	DataRes	WxData	Fire Behavior Model	Burned (Agreement)	Underpredicted (Error)	Overpredicted (Error)	Unburned (Agreement)	Total Area	Total Agreement
cust	30m	che	HFIRE	2584	1631	8381	19482	32078	22066
cust	30m	che	FARSITE	2734	1481	8341	19523	32079	22257
cust	100m	che	HFIRE	2439	1786	6732	21158	32115	23597
cust	100m	che	FARSITE	3125	1100	9165	18725	32115	21850
cust	30m	mal	HFIRE	3736	479	13079	14785	32079	18521
cust	30m	mal	FARSITE	4059	156	14717	13147	32079	17206
cust	100m	mal	HFIRE	3666	559	10941	16949	32115	20615
cust	100m	mal	FARSITE	4165	60	15059	12831	32115	16996
nffl	30m	che	HFIRE	4007	8	8883	11344	24242	15351
nffl	30m	che	FARSITE	3907	108	7783	12444	24242	16351
nffl	100m	che	HFIRE	3995	20	8124	12140	24279	16135
nffl	100m	che	FARSITE	3998	17	8442	11822	24279	15820
nffl	30m	mal	HFIRE	4000	15	7240	12986	24241	16986
nffl	30m	mal	FARSITE	4008	7	8192	12034	24241	16042
nffl	100m	mal	HFIRE	3774	241	6226	14038	24279	17812
nffl	100m	mal	FARSITE	4003	12	11289	8975	24279	12978
cust	30m	-	Historical	4215	0	0	27863	32078	32078
cust	100m	-	Historical	4225	0	0	27890	32115	32115
nffl	30m	-	Historical	4015	0	0	20226	24241	24241
nffl	100m	-	Historical	4015	0	0	20264	24279	24279

Table F.2. Measures of Association For Observed and Predicted Fire Spread During the 1996 Calabasas Fire

Duration of 1996 Calabasas Simulation: 10/21 1100 to 10/21 2100 (10 hours)				<i>kappa</i>	<i>conditional kappa</i>	<i>conditional kappa</i>	<i>chi squared</i>	<i>Jacard's</i>	<i>areal association</i>
FuelsUsed	DataRes	WxData	Fire Behavior Model	κ	κ_{burn}	κ_{unburn}	χ^2	C_J	C_A
cust	30m	che	HFIRE	0.1859	0.4121	0.1200	1586.6980	0.2051	0.6879
cust	30m	che	FARSITE	0.2066	0.4634	0.1329	1975.9954	0.2177	0.6938
cust	100m	che	HFIRE	0.2244	0.4083	0.1547	2029.1802	0.2226	0.7348
cust	100m	che	FARSITE	0.2271	0.5782	0.1413	2624.0405	0.2334	0.6804
cust	30m	mal	HFIRE	0.1838	0.7612	0.1045	2552.1653	0.2160	0.5774
cust	30m	mal	FARSITE	0.1763	0.9108	0.0976	2851.8178	0.2144	0.5364
cust	100m	mal	HFIRE	0.2328	0.7573	0.1375	3344.3065	0.2417	0.6419
cust	100m	mal	FARSITE	0.1779	0.9646	0.0980	3035.5849	0.2160	0.5292
nffl	30m	che	HFIRE	0.2963	0.9957	0.1741	4201.8278	0.3107	0.6332
nffl	30m	che	FARSITE	0.3331	0.9480	0.2021	4643.8965	0.3312	0.6745
nffl	100m	che	HFIRE	0.3284	0.9901	0.1968	4731.2496	0.3291	0.6646
nffl	100m	che	FARSITE	0.3145	0.9913	0.1869	4498.9457	0.3209	0.6516
nffl	30m	mal	HFIRE	0.3709	0.9930	0.2280	5488.6409	0.3554	0.7007
nffl	30m	mal	FARSITE	0.3265	0.9965	0.1952	4716.0103	0.3283	0.6618
nffl	100m	mal	HFIRE	0.3960	0.8979	0.2540	5538.3649	0.3685	0.7336
nffl	100m	mal	FARSITE	0.2069	0.9919	0.1155	2781.6328	0.2616	0.5345
cust	30m	-	Historical	1.0000	1.0000	1.0000	32078.0000	1.0000	1.0000
cust	100m	-	Historical	1.0000	1.0000	1.0000	32115.0000	1.0000	1.0000
nffl	30m	-	Historical	1.0000	1.0000	1.0000	24241.0000	1.0000	1.0000
nffl	100m	-	Historical	1.0000	1.0000	1.0000	24279.0000	1.0000	1.0000

APPENDIX G: 1998 OGILVY FIRE SIMULATION: RAW RESULTS

Table G.1 shows the area totals at the conclusion of 89 hours of the 1998 Ogilvy Fire. These totals were used to generate the measures of association used to evaluate the accuracy of the HFire and FARSITE models. Although not reported in the main body of the text, additional measures of association other than C_J , C_A , and κ were calculated using the data in Table G.1. The values of the additional coefficients appear in Table G.2.

Table G.1. Correspondence Table For Observed and Predicted Fire Spread During the 1998 Ogilvy Fire

Duration of 1998 Ogilvy Fire Simulation: 10/16 1500 to 10/20 0800 (89 hours)				ha	ha	ha	ha	ha	ha
FuelsUsed	DataRes	WxDData	Fire Behavior Model	Burned (Agreement)	Underpredicted (Error)	Overpredicted (Error)	Unburned (Agreement)	Total Area	Total Agreement
cust	30m	-	HFIRE	1421	2	23755	42937	68115	44358
cust	30m	-	FARSITE	1423	0	34684	32008	68115	33431
cust	100m	-	HFIRE	1420	2	10487	56225	68134	57645
cust	100m	-	FARSITE	1422	0	34854	31858	68134	33280
nffl	30m	-	HFIRE	1423	0	63783	2909	68115	4332
nffl	30m	-	FARSITE	1423	0	66559	133	68115	1556
nffl	100m	-	HFIRE	1422	0	60440	6272	68134	7694
nffl	100m	-	FARSITE	1422	0	66709	3	68134	1425
cust	30m	-	Historical	1423	0	0	66692	68115	68115
cust	100m	-	Historical	1422	0	0	66712	68134	68134
nffl	30m	-	Historical	1423	0	0	66692	68115	68115
nffl	100m	-	Historical	1422	0	0	66712	68134	68134

Table G.2. Measures of Association For Observed and Predicted Fire Spread During the 1998 Ogilvy Fire

Duration of 1998 Ogilvy Fire Simulation: 10/16 1500 to 10/20 0800 (89 hours)				<i>kappa</i>	<i>conditional kappa</i>	<i>conditional kappa</i>	<i>chi squared</i>	<i>Jacard's</i>	<i>areal association</i>
FuelsUsed	DataRes	WxData	Fire Behavior Model	κ	κ_{burn}	κ_{unburn}	χ^2	C_J	C_A
cust	30m	-	HFIRE	0.0701	0.9978	0.0363	2467.7457	0.0564	0.6512
cust	30m	-	FARSITE	0.0371	1.0000	0.0189	1288.3713	0.0394	0.4908
cust	100m	-	HFIRE	0.1826	0.9983	0.1005	6834.7159	0.1192	0.8461
cust	100m	-	FARSITE	0.0368	1.0000	0.0187	1275.4359	0.0392	0.4884
nffl	30m	-	HFIRE	0.0019	1.0000	0.0010	64.8381	0.0218	0.0636
nffl	30m	-	FARSITE	0.0001	1.0000	0.0000	2.8434	0.0209	0.0228
nffl	100m	-	HFIRE	0.0043	1.0000	0.0022	147.2454	0.0230	0.1129
nffl	100m	-	FARSITE	0.0000	1.0000	0.0000	0.0639	0.0209	0.0209
cust	30m	-	Historical	1.0000	1.0000	1.0000	68115.0000	1.0000	1.0000
cust	100m	-	Historical	1.0000	1.0000	1.0000	68134.0000	1.0000	1.0000
nffl	30m	-	Historical	1.0000	1.0000	1.0000	68115.0000	1.0000	1.0000
nffl	100m	-	Historical	1.0000	1.0000	1.0000	68134.0000	1.0000	1.0000